UNIVERSITY OF OKLAHOMA

GRADUATE COLLEGE

MEASURING THE TRILINEAR HIGGS COUPLINGS AT LHC

A DISSERTATION

SUBMITTED TO THE GRADUATE FACULTY

in partial fullfillment of the requirements for the

degree of

DOCTOR OF PHILOSOPHY

By

PRIYANGIKA WICKRAMARACHCHI
Norman, Oklahoma
2015

Measuring the Trilinear Higgs Couplings at LHC

A Dissertation Approved for the
Homer L. Dodge Department of Physics and Astronomy

By

_____

Dr. Chung Kao, Chair

_____

Dr. Nikola Petrov

_____

Dr. Deborah Watson

_____

Dr. Ron Kantowski

_____

Dr. Howie Baer

කුඩා කල සිට මා ළඟින් සිට

දහසක් කැපකිරීම් මැද

මා දිරිමත් කළ

මගේ ආදරණීය දෙමාපියන්ට

සෙනෙහසින් පිළිගැන්වෙයි ...

This dissertation is dedicated to my loving parents,

who always encouraged me to pursue higher education and

dedicated their lives for our future...

Acknowledgements

I would like to express my deepest gratitude to my thesis advisor Professor Chung Kao for his continual guidance, encouragement and support throughout my PHD. Thank you for being a good teacher and an excellent and understanding mentor. My sincere gratitude to the rest of my thesis committee, Dr. Nikola Petrov from the Department of Mathematics, Dr. Deborah Watson, Dr. Howie Baer and Dr. Ron Kantowski from the Homer L. Dodge Department of Physics and Astronomy, for their important suggestions and encouragement throughout the years. I would also like to thankfully remember Dr. Darryl McCullough from the Math Department who sat on my committee until his retirement in 2011.

My sincere thanks to Dr. Joshua Sayre who was a post doctoral researcher in our group until 2012, for his support when I was first beginning this research. Dr. Kesheng Yang, who was a graduate student when I joined the group, thank you so much for your enormous support from the beginning. I would not be at this position today without your support. I also wish to thank, postdoctoral researcher, Dr. Baris Altukaynak for his support. I specially want to thank Mr Brent McCoy, for the enormous help given for corrections of the thesis. Your help is really appreciated.

I would like to convey my gratitude to Dr. Kieran Mullen and Dr. Kimball Milton for being really helpful and responsible faculty as graduate liasons. I also would like to acknowledge all faculty and staff from the Hormer L. Dodge Department of Physics and Astronomy, for their generous help.

Many thanks to all Srilankan friends who are and were in Norman, your help is

Table of Contents

List of Tables

List of Figures

Abstract

The results from the Large Hadron Collider (LHC) indicate that the couplings of the Higgs boson to other particles are consistent with the Standard Model. The coupling of the Higgs boson to itself will be the final and ultimate test as to whether this particle is the standard Higgs boson. Both the trilinear Higgs coupling as well as the quartic coupling is needed in order to verify the Higgs potential accurately. Our goal is to determine how well the trilinear Higgs coupling can be determined theoretically. We study the Higgs pair production from gluon fusion at the LHC in the Standard Model and Minimal Supersymmetric Standard Model. We consider the collider energy of the LHC Run 2 with $\sqrt{s} = 13$ TeV and 14 TeV to study the production rate of Higgs boson pairs and physics background for final states; $hh \to b\bar{b}b\bar{b}$ and $hh \to b\bar{b}\tau^+\tau^-$ with realistic acceptance cuts.

Chapter 1

Introduction

1.1 Discovery of the Higgs Boson

The existence of a boson with mass 125 GeV was first announced on 4 of July 2012 by ATLAS and CMS at the Large Hadron Collider (LHC), and physicists suspected at the time that it was the Higgs boson. This particle had been proven to behave, interact and decay as predicted by the Standard Model (SM). In March 2013, it was tentatively confirmed as the Higgs boson.

In October 2013, the Royal Swedish Academy of Sciences awarded the 2013 Nobel prize in Physics, jointly, to Francois Englert and Peter W. Higgs for the, *"theoretical discovery of a mechanism that contributes to our understanding of the origin of mass of subatomic particles and which recently was confirmed through the discovery of the predicted fundamental particle, by the ATLAS and CMS experiments at CERN's Large Hadron Collider."* [2]

The mass of the SM Higgs boson has been measured to good precision by the ATLAS [3] and CMS [4] collaborations at the LHC. These measurements have been made using proton-proton (pp) collision data at $\sqrt{s} = 7$ TeV and at $\sqrt{s} = 8$ TeV. More precise measurements of Higgs production, decay rates, couplings, masses, new decay modes, measurements of Higgs self coupling and additional Higgs bosons beyond the Standard Model are expected in LHC Run2 which is currently $\sqrt{s} = 13$ TeV and will be upgraded to $\sqrt{s} = 14$ TeV in the future.

1.2 Standard Model

The Standard Model is a gauge theory which combines all three fundamental interactions strong, weak and electromagnetic. The electroweak interaction is described by the $SU(2)_L \otimes U(1)_Y$ group while QCD is an SU(3) Yang Mills theory [5]. Since the mass terms of gauge bosons violate the gauge invariance of $SU(2)_L \otimes U(1)_Y$ theory, the masses are set to be zero, though in reality they are observed to have mass. This led theorists to introduce a realistic and renormalizable mechanism to give masses to fermions and gauge bosons. Though it is often called the Higgs Mechanism, several groups also contributed to the development of this mechanism in 1964, [6][7][8]. Therefore, in history, it is called Englert-Brout-Higgs-Guranlik-Hagen-Kibble mechanism which explains how the vector bosons acquire non zero masses through spontaneous symmetry breaking.
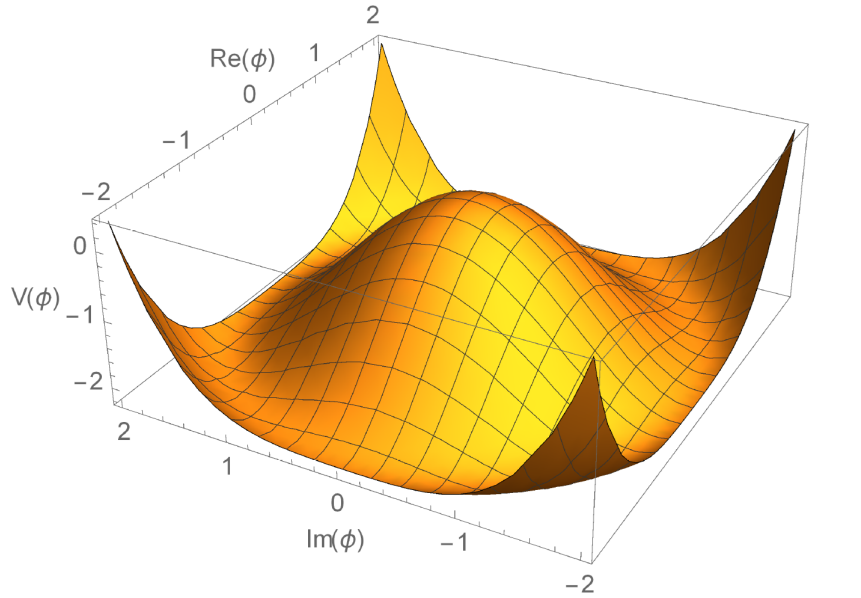
Figure 1.1: 3D plot of Higgs potential vs Real and Imaginary parts of complex Φ.

The Higgs potential can be written as,

$$V(\Phi) = -\mu^2 \Phi^\dagger \Phi + \lambda(\Phi^\dagger \Phi)^2 \tag{1.1}$$

Fig. 1.1 shows a plot of Higgs potential; $\Phi = 0$ is an unstable maximum while its minimum is at $\Phi = \sqrt{\mu^2/2\lambda}$.

The Higgs sector of the Standard Model Lagrangian can be written as,

$$\mathcal{L}_H = (\mathcal{D}^\mu \Phi)^\dagger (\mathcal{D}_\mu \Phi) + \mu^2 \Phi^\dagger \Phi - \lambda(\Phi^\dagger \Phi)^2 \tag{1.2}$$

$$\mathcal{D}^\mu = \partial^\mu + ig\frac{\tau_j}{2}W_j^\mu + ig'\frac{Y}{2}B^\mu \tag{1.3}$$

$\lambda > 0$ and $\mu^2 > 0$, Y is weak hyper-charge and +1 for the Higgs field, or can be written in matrix form $Y = \begin{pmatrix} 1 & 0 \\ 0 & 1 \end{pmatrix}$.

$\tau_j = \frac{1}{2}\sigma_j$ and σ_j denotes the Pauli matrices,

$$\sigma_1 = \begin{pmatrix} 0 & 1 \\ 1 & 0 \end{pmatrix} \quad,\quad \sigma_2 = \begin{pmatrix} 0 & -i \\ i & 0 \end{pmatrix} \quad,\quad \sigma_3 = \begin{pmatrix} 1 & 0 \\ 0 & -1 \end{pmatrix}$$

and $B(x)$ is the gauge boson corresponding to the $U(1)_Y$ group. This Lagrangian is invariant under $SU(2)_L \otimes U(1)_Y$ gauge transformations. Φ is the Higgs field and is given by,

$$\Phi = \begin{pmatrix} \phi_a \\ \phi_b \end{pmatrix} = \frac{1}{\sqrt{2}} \begin{pmatrix} 0 \\ v + h(x) \end{pmatrix} \tag{1.4}$$

where, $v = \sqrt{\mu^2/\lambda} = 246\,GeV$, is the vacuum expectation value (vev). Incorporating all these facts, the Higgs Lagrangian changes to a form containing terms that give masses to the gauge bosons; $m_W = gv/2$ and $m_Z = gv/2\,cos\theta_w$. Fermion masses

3

come from the same mechanism with Yukawa part of the Lagrangian; $m_i = \lambda_i \, v/\sqrt{2}$ where $i = e, u, d$, and λ_i are Yukawa couplings. In the SM, neutrinos do not interact with the Higgs boson so they are massless. The mass of the Higgs boson is a free parameter in the SM and is given by $M_H = \sqrt{2\lambda v^2} = \sqrt{2\mu^2}$. This is called the well known Higgs mechanism.

1.3 Physics beyond the Standard Model

Even though the SM gives the currently available, well tested, best description for the subatomic world, there are topics, that cannot be explained by this theory. The parameters in the SM like masses, mixing and couplings for leptons and quarks are experimentally proven. The SM also does not provide explanations for cosmological parameters such as dark matter and dark energy. Having all these unanswered questions, it is clear that the SM does not give a complete picture about the subatomic world and the universe. So one might say the Standard Model is a small part of a bigger story that explains the whole world. Furthermore, the SM does not show a grand unification of strong and electroweak forces at very high energy scale indicating the necessity of a theory beyond the SM. Supersymmetry provides solutions for most of these questions by introducing a super partner for every particle. In supersymmetry, super partners for each particle in the SM whose spin differs by a $1/2$ are introduced as well as both particle and its super partner should have the same transformation properties under the $SU(3)_C \times SU(2)_L \times U(1)_Y$ gauge group [9] [1]. It also unifies the three forces weak, strong and electromagnetic. Fig. 1.2 shows the behavior of three

forces for high energies in the Standard Model as well as Minimal Supersymmetric

Standard Model (MSSM).
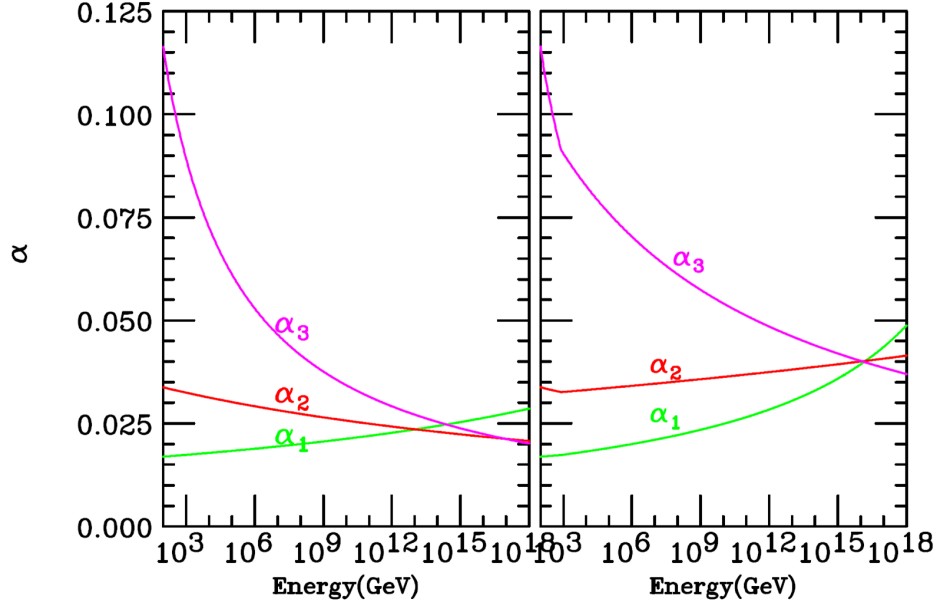
Figure 1.2: Three Gauge Couplings a) in the SM b) for the MSSM (generated using Isajet 7.8.1). Red curve represents the gauge coupling of $SU(2)_L$. Green curve is for the gauge coupling of $U(1)_Y$, and color magenta represents strong $SU(3)_C$ interaction.

1.4 Minimal Supersymmetric Standard Model

Some of the unanswered questions in the SM can be explained introducing two Higgs doublets instead of a single Higgs doublet in the SM. Therefore, in the supersymmetric models, two Higgs doublets are needed to give masses to both up-type and down-type quarks and the corresponding leptons[1] [10] [11]. There are three famous subcatagories in the two Higgs doublet models (2HDM) based on their couplings to leptons. In Type

1, one doublet couples to both up-and down type fermions whereas the other does not couple to any fermions [12] [13]. In Type II, one doublet(Φ_1) couples to down flavor while the other doublet(Φ_2) couples to up flavor fermions [14] [15] [13] and in Type III, both doublets couple to both up and down flavored fermions. The MSSM is Type II two Higgs doublet model which is considered to be the minimal extension to the Standard Model. The MSSM has a second complex SU(2) Higgs-doublet field with hypercharge $Y = -1$ and both doublets acquire vacuum expectation values to break the $SU(2)_L \times U(1)_Y$ symmetry. The general form of the Higgs potential for 2HDM can be written as,

$$V_{Higgs}(\phi_1, \phi_2) = m_1^2 \phi_1^\dagger \phi_1 + m_2^2 \phi_2^\dagger \phi_2 + m_{12}^2(\phi_1^\dagger \phi_2 + \phi_2^\dagger \phi_1) + \lambda_1(\phi_1^\dagger \phi_1)^2 + \lambda_2(\phi_2^\dagger \phi_2)^2$$

$$+ \lambda_3(\phi_1^\dagger \phi_1)(\phi_2^\dagger \phi_2) + \lambda_4[(\phi_1^\dagger \phi_2)(\phi_2^\dagger \phi_1)] + \lambda_5[(\phi_1^\dagger \phi_2)^2 + (\phi_2^\dagger \phi_1)^2] \quad (1.5)$$

where Φ_1 and Φ_2 are two doublets in the Higgs sector of 2HDM which are,

$$\Phi_1 = \begin{pmatrix} 0 \\ v_1 \end{pmatrix} \qquad \Phi_2 = \begin{pmatrix} v_2 \\ 0 \end{pmatrix}$$

v_1 and v_2 are vacuum expectation values in the Higgs field, $v = \sqrt{v_1^2 + v_2^2} \approx 246\ GeV$, and there is no CP violation in the Higgs sector. In the 2HDM Higgs potential, there are 8 unknowns namely m_1, m_2, m_{12}, λ_1, λ_2, λ_3, λ_4 and λ_5 all of which are real in this case. Three of them are Goldstone modes and are absorbed by $W^\pm$ and Z bosons. The remaining five degrees of freedom lead to the five physical Higgs bosons of the MSSM. In these five, two are CP even neutral Higgs bosons, the h^0(lighter) and

H^0(heavier), one CP odd neutral pseudo scalar A^0 and a pair of singly charged Higgs bosons $H^{\pm}$, and these lead to a large variety of self couplings among them. At tree level, Higgs boson masses and couplings of the MSSM Higgses are determined by two free parameters, the mass of the CP odd pseudo scalar (m_A) and the ratio of vacuum expectation values ($tan\beta = v_1/v_2$) where $0 \leq \beta \leq \frac{\pi}{2}$. Higgs self couplings as well as tree level Higgs-Fermion Yukawa couplings are given in the appendix of this thesis.

1.5   Outline

After the discovery of Higgs, now it is necessary to investigate its properties to verify that it is exactly the SM Higgs boson. Towards this goal, measurement of Higgs self coupling is really important to reproduce the correct Higgs potential, and this will be focused on the next runs at the LHC. Our main focus in this study is to explore the possibilities of measuring the trilinear Higgs couplings in future experiments. We first study the dominant Higgs production processes which provide a way to measure the Higgs coupling. Gluon fusion is the dominant source of Higgs boson pair production via box and triangle diagrams, and it has been studied by several groups in the past [16],[17],[18],[19] and [20]. The distructive interference between two diagrams provides a path to measure the trilinear Higgs couplings at the LHC. Chapter 2 of this thesis discusses the production cross section of the Higgs bosons via gluon fusion at the LHC. Once Higgs bosons are produced, they will decay into other particles such as quarks, tau leptons, W and Z bosons and so on. The branching ratio of Higgs decays provides important facts that allow us to choose probable decay channels. Fig. 1.3

shows the branching ratios for the Standard Model Higgs, and Fig. 1.4 shows the branching ratios of the MSSM pseudo scalar for two different $tan\,\beta$ values. It is clear that the Higgs dominantly decays into $b\bar{b}$ pair both in the SM (for Higgs mass of 126 GeV) as well as in MSSM for high $tan\beta$ regions. The second highest rate of decay is $h^0 \rightarrow \tau^+\tau^-$.
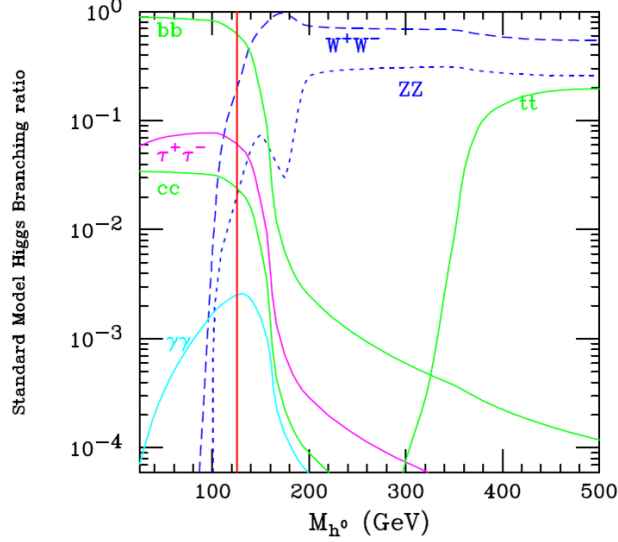
Figure 1.3: Branching Ratio for SM Higgs.

Though $b\bar{b}$ is the dominant decay mode for the neutral Higgs, not many studies have been conducted because the signal is overwhelmed by QCD backgrounds unless a special triggering is selected. We study the production cross sections for the process $gg \rightarrow \phi^0\phi^0 \rightarrow b\bar{b}b\bar{b}$, $gg \rightarrow \phi^0\phi^0 \rightarrow b\bar{b}\tau^+\tau^-$ and $\tau^\pm \rightarrow l, j_\tau$ for both the SM and the MSSM in Chapter 2. In the MSSM, the Yukawa coupling is enhanced by large value of $tan\,\beta$ and therefore Higgs production by b quarks plays a major role here. In Chapter 3, Higgs cross sections for the processes $b\bar{b} \rightarrow \phi^0\phi^0 \rightarrow b\bar{b}b\bar{b}$ and $b\bar{b} \rightarrow \phi^0\phi^0 \rightarrow b\bar{b}\tau^+\tau^-$ and $\tau^\pm \rightarrow l, J_\tau$ are discussed. The choice of selection cuts and numerical results for
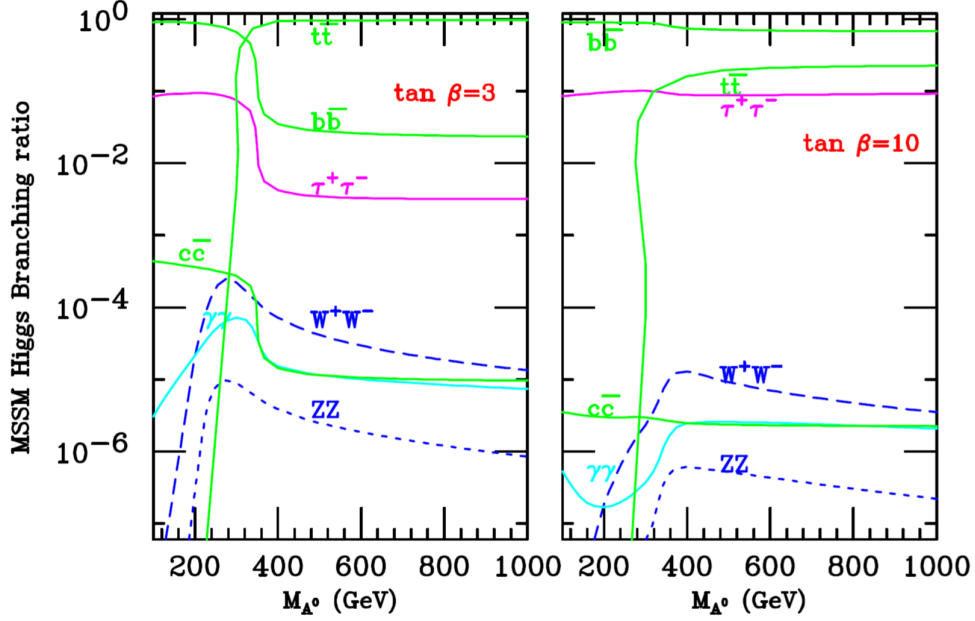
Figure 1.4: Branching Ratio for the MSSM pseudoscalar Higgs (a) with

$tan \ \beta \ = 3$ and (b) with $tan \ \beta \ = 10$.

several distributions is presented in 'Calculation tools'. The dominant Standard Model

background for the mentioned processes was discussed in Chapter 4 with analysis of

statistical significance. Chapter 5 includes a discussion about measuring the trilinear

Higgs coupling at the LHC via the Higgs production processes discussed in Chapter 2

and 3. However, measuring the Higgs self coupling is not an easy task at the LHC due

to small cross sections and large backgrounds in the $gg \rightarrow hh$ process. Lepton colliders

are well known for high precision measurements and measuring the trilinear Higgs

coupling will be one of the main focuses of next e^+e^- machine that has been proposed,

International Linear collider(ILC). The trilinear Higgs self coupling is discussed in

Chapter 6, for the production of the SM Higgs at ILC via e^+e^- collisions.

Chapter 2

Higgs Production Through Gluon Fusion

Gluon fusion is one of the most promising production channels for Higgs bosons at the LHC, and therefore the calculations of production cross sections for this process have been of great interest. As discussed in Chapter 1, in the Standard Model gluon fusion is the dominant channel to produce a pair of Higgs bosons through a quark loop of triangle and box. Even beyond the SM, in the MSSM, gluon fusion is the major source of neutral Higgs bosons at the LHC for lower values of $tan\beta$. This chapter presents a study of the production of neutral Higgs bosons with a gluon pair via quark loop followed by (a) Higgs decays into two pairs of bottom quarks ($gg \rightarrow \phi^0\phi^0 + X \rightarrow b\bar{b}b\bar{b} + X$) and (b) One Higgs decays into a $b\bar{b}$ pair and the other Higgs decays into leptons ($gg \rightarrow \phi^0\phi^0 + X \rightarrow b\bar{b}\tau^+\tau^- + X \rightarrow b\bar{b}lj_\tau + \not{E}_T + X$). These processes were studied in the SM for the Higgs that has already been discovered with a mass 125.0 GeV and in the MSSM for the three neutral Higgses h^0, H^0 or A^0 in the mass region of $100 - 1000$ GeV.

2.1 Two Higgs Production

Fig. 2.1 represents the diagrams contributing to pair production of SM Higgs bosons via the gluon fusion process $gg \rightarrow hh$. As can be seen from the Fig. 2.1, gluon fusion has contributions from the virtual box diagram and the virtual triangle diagram. In the triangle diagram, an off shell Higgs is produced and decays into two real Higgses

via the three Higgs self couplings.
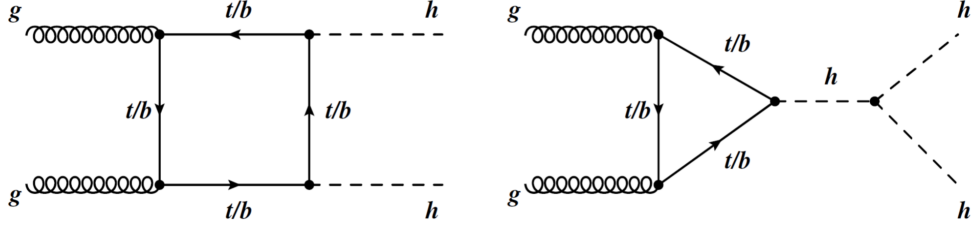
Figure 2.1: Generic diagrams contributing to pair production of SM Higgs bosons in gluon-gluon collisions (left) via box diagram and (right) via triangle diagrams.

2.2 Calculation tools for the signal

The cross section of two Higgs production at LHC via gluon fusion was evaluated with center of mass energy $\sqrt{s} = 14$ TeV. This process includes box and triangle diagrams given in Fig. 2.1 on the order of α_s^2. Along the box and triangle loops, the intermediate fermions are massive third generation quarks. The Yukawa couplings given in Appendix B were calculated using quark masses of $m_t = 173.1$ GeV and $m_b = 4.7$ GeV. For the calculation of strong coupling, the renormalization scale is set to be $\mu_R = \sqrt{\hat{s}}$, which is the parton center of mass energy. The signal cross sections were computed using MSTW2008 [21] parton distribution functions(pdfs) with the factorization scale $\mu_F = \sqrt{\hat{s}}$. The transition amplitudes for loops were calculated using a tensor reduction procedure explained by Passarino and Veltmann [22]. All tensors were reduced to scalar integrals in terms of D_0, C_0, B_0 and A_0 using FORM [23]. Two Higgs signals were generated using a Monte Carlo program with the amplitudes

calculated by FORM. In order to include the higher order corrections, the results were multiplied by a K factor. K factors for $E_{CM} = 14$ TeV were calculated using the formulas given in [20],

$$\frac{\sigma_{NNLO}}{\sigma_{NLO}} = 1.149 - 0.326 \left(\frac{E_{CM}}{1\ TeV}\right)^{-1} + 0.327 \left(\frac{E_{CM}}{1\ TeV}\right)^{-\frac{1}{2}} \tag{2.1}$$

$$\frac{\sigma_{NNLO}}{\sigma_{LO}} = 1.242 - 7.17 \left(\frac{E_{CM}}{1\ TeV}\right)^{-1} + 5.77 \left(\frac{E_{CM}}{1\ TeV}\right)^{-\frac{1}{2}} \tag{2.2}$$

The above discussed tools were used throughout this chapter unless otherwise specifically mentioned in each section.

2.3 Numerical Results

2.3.1 Standard Model Higgs : $gg \longrightarrow hh$

In Fig. 2.1, h is SM Higgs with mass 125.5 GeV. The production cross section is calculated for SM Higgs, and the individual contributions from triangle diagram and box diagrams and the total cross sections are presented in Table 2.1. The results were also compared with the cross sections presented in Florian et.al [20] and found to agree within the uncertainty. As we can see from the results, the contribution from box diagrams are much larger than the total because the triangle and box diagrams interfere destructively. The next to the leading order(NLO) cross section for the production of SM Higgs pairs via gluon fusion was calculated with a K factor of 1.88 for $\sqrt{s} = 14$ TeV, and the results were compared to the cross sections presented in recent studies. See Table 2.2 for numerical values.

Contribution	$M_h = 125.5$ GeV
TRIANGLE	5.16
BOX	37.8
TOTAL	17.9

Table 2.1: Leading order cross section in fb for Standard Model Higgs pair production via gluon fusion for the LHC running at 14 TeV.

Reference	$\sigma_{NLO}^{gg \to hh}$ fb
Florian et.al[20]	33.2
Baglio et.al [24]	33.89
This study	33.6

Table 2.2: Next to the leading order(NLO) cross section in fb for Standard Model Higgs pair production via gluon fusion at the LHC for 14 TeV.

2.3.2 Higgs decay into $b\bar{b}$

Each Higgs produced here decays into $b\bar{b}$. The cross section for $pp \to (h \to b\bar{b})(h \to b\bar{b})$ was calculated using the Narrow Width Approximation (NWA) so that

$$\sigma(pp \to \phi^0\phi^0 \to b\bar{b}b\bar{b} + X) = \sigma(pp \to \phi^0\phi^0 + X) \times B(\phi^0 \to b\bar{b}) \times B(\phi^0 \to b\bar{b}) \quad (2.3)$$

where $B(\phi^0 \to b\bar{b})$ is the branching fraction of the Higgs boson decaying into $b\bar{b}$. We also applied the basic acceptance cuts for the final states at LHC with integrated luminosity $L = 30 \ fb^{-1}$ and $\sqrt{s} = 14$ TeV. High Transverse momentum (P_T) trigger is

required by LHC detectors for the final state b quarks. Here we apply $P_T(b) > 25\,GeV$ for the transverse momentum of final state b quarks. Fig. 2.2 represents the transverse-momentum distribution of the final state bottom quarks $(b\,or\,\bar{b})$ and as can be seen in the Fig. 2.2, the bottom quarks are ordered according to their transverse momenta, $p_T(b_1) \geq P_T(b_2) \geq P_T(b_3) \geq P_T(b_4)$.
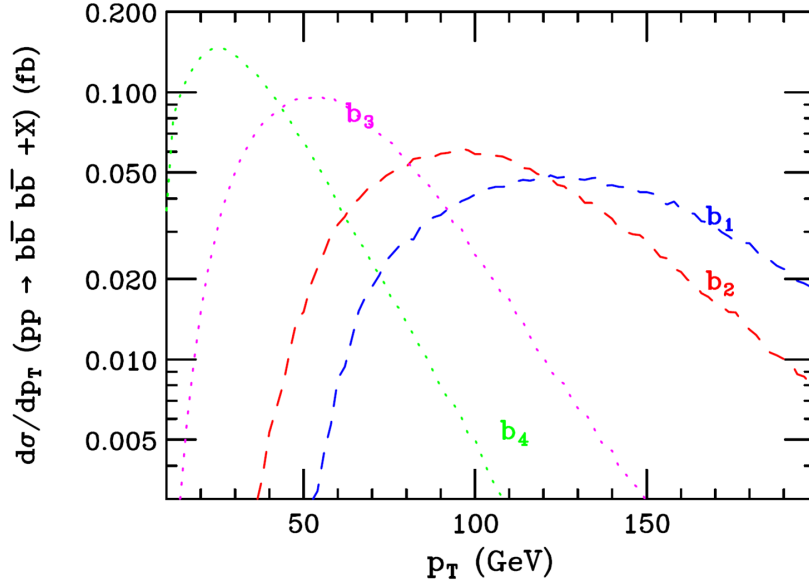
Figure 2.2: The transverse momentum distribution for the final b quarks produced, generating the SM Higgs signal from $pp \to hh \to b\bar{b}b\bar{b}$.

The pseudorapidity(η) for light particles can be defined as,

$$\eta = -ln\left[tan\left(\frac{\theta}{2}\right)\right]$$

where, θ is the angle between the outgoing particle and the beam axis. For final state b quark here, we chose $|\eta_b| < 2.5$.

We also introduce a special mass cut here to save the signal from high QCD backgrounds. b_1 is the final state b which has the highest transverse momentum, and the

next three jets were re ordered so that the second jet minimizes, $\Delta M_{1j} = |M_{1j} - M_\phi|$ where $j = 2, 3, 4$. According to this, two selected pairs(12 and 34) of the final state b should require $|M_{b\bar{b}} - M_\phi| \leq \Delta M_{bb}$ where $\Delta M_{bb} = 0.15 M_\phi$. Fig. 2.3 shows the invariant-mass($M_{ij}, i, j = 1, 2, 3, 4$) distribution of the final state $b_i b_j$ pairs for the Higgs signal $pp \rightarrow b\bar{b}\, b\bar{b} + X$ via $gg \rightarrow hh$ after reordering jets.
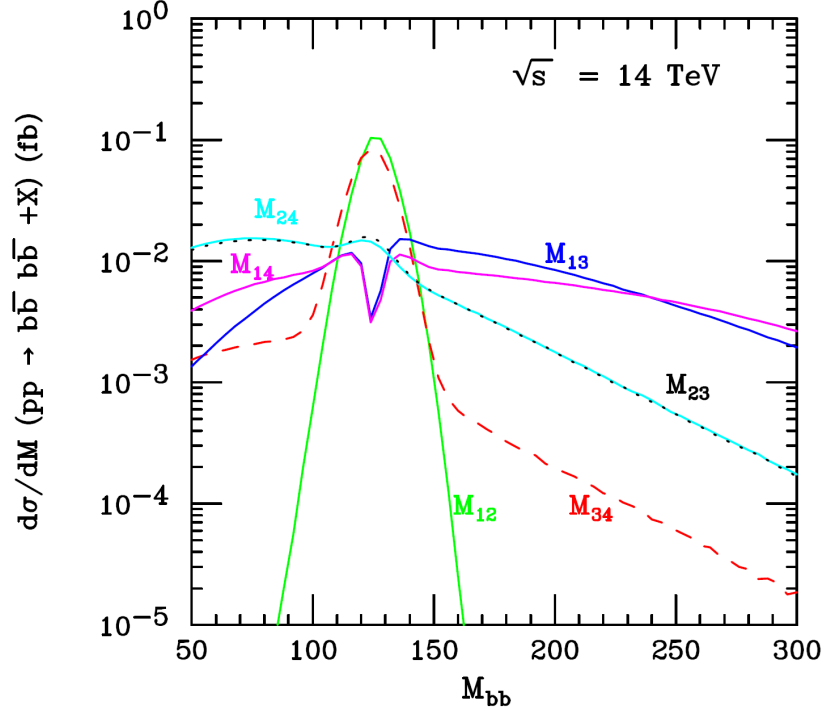
Figure 2.3: The invariant mass distribution for the Higgs signal from $gg \rightarrow hh \rightarrow b\bar{b}\, b\bar{b} + X$ with $M_h = 125.5$ GeV.

For the angle between the final state particles, we used, $\Delta R > 0.4$, where ΔR is defined by,

$$\Delta R = \sqrt{(\Delta\Phi)^2 + (\Delta\eta)^2} \tag{2.4}$$

where Φ is the angle between two particles in the transverse plane. Finally the

Gaussian smearing given below (in GeV) was applied to the outgoing momentum to approximate the detector effects.

$$\frac{\Delta E}{E} = \frac{0.5}{\sqrt{E}} \oplus 0.03 \tag{2.5}$$

Table 2.3 presents the calculated cross section for the signal $pp \to b\bar{b}b\bar{b}$ via $gg \to hh$ for the SM Higgs of mass 125.5 GeV. Appropriate branching ratio is also given in the table.

Cross section in fb	$M_h = 125.5$ GeV
$\sigma(gg \to hh \to 4b)$	3.40
BF_{bb}	0.626

Table 2.3: LO cross section in fb for $gg \to hh \to b\bar{b}b\bar{b} + X$ for the Standard Model using pdfs from MSTW2008. BF_{bb} is the branching ratio of Higgs decaying into $b\bar{b}$.

2.3.3   Higgs decay into $\tau^+ \tau^-$

In the Standard Model, the Higgs dominantly decays into $b\bar{b}$ with branching ratio $\approx 60\%$, into WW^* with branching ratio $\approx 22\%$ and into $\tau^+\tau^-$ with branching ratio $\approx 6\%$. In this study we also considered the production of a Higgs pair via gluon fusion followed by one Higgs decaying into $b\bar{b}$ while the other decays into a pair of τ, τ^+ and τ^- which decays into lighter leptons($e^\pm$ or $\mu^\pm$), mesons($\pi/a_1/\rho$) and missing energy. The mass of the Higgs boson is much heavier than the mass of the tau leptons, and

therefore the two leptons are very energetic. Hence, for the decay of tau here we use the Collinear Approximation which assumes the final particles from tau decay are almost along the same direction as its parent particles. Except for the basic cuts applied for final state $b\bar{b}$ which is explained in the previous section, we use,

$$P_T(j) > 15\,GeV, \quad P_T(l) > 20\,GeV, \quad P_T(j_\tau) > 40 GeV$$

$$|\eta(j)| < 2.5, \qquad |\eta(l)| < 2.5, \qquad |\eta(j_\tau)| < 2.5 \qquad (2.6)$$

$$\Delta R(jj_\tau) > 0.4, \qquad \Delta R(lj_\tau) > 0.4, \qquad \Delta R(lj) > 0.4$$

$$\not{E}_T > 40\,GeV, \quad m_T(l, \not{E}_T) < 30\,GeV, \quad \phi(l, j_\tau) < 170^0$$

$\not{E}_T$ is the missing transverse energy, and $\phi(l, j_\tau)$ is the transverse angle between lepton and tau jet. The quantity $m_T(l, \not{E}_T)$ is the transverse mass of lepton and neutrino as defined in "*Collider Physics*"[25]. Gaussian smearing in GeV, for charged leptons used here can be given by,

$$\frac{\Delta E}{E} = \frac{0.25}{\sqrt{E}} \oplus 0.01. \qquad (2.7)$$

Table 2.4 gives the calculated LO cross sections for the process $gg \to hh \to b\bar{b}\tau^+\tau^-$ followed by $\tau^+\tau^- \to lj_\tau + \not{E}_T$.

2.4 Production of MSSM Higgs

The mechanisms for the production of two MSSM Higgs bosons are similar to the SM, and the possible diagrams are given in Fig. 2.4. Though several combinations

Cross section in fb	$M_h = 125.5$ GeV
$\sigma(pp \to hh \to bb\tau^+\tau^- \to b\bar{b}lj_\tau + \not{E}_T)$	0.0613

Table 2.4: LO cross section in fb for $gg \to hh \to b\bar{b}\tau^+\tau^- \to b\bar{b}lj_\tau + \not{E}_T + X$ for the Standard Model using pdfs from MSTW2008.

of neutral Higgs pairs of the MSSM can be produced through gluon fusion, here we consider the processes $pp \to h^0h^0/H^0H^0/A^0A^0$ where h^0 and H^0 are CP even light and heavy Higgs bosons in the MSSM respectively, and A^0 is CP odd pseudo scalar. The intermediate virtual Higgs boson in the triangle diagram should be either h^0 or H^0 to preserve the CP conservation at the three Higgs vertex.
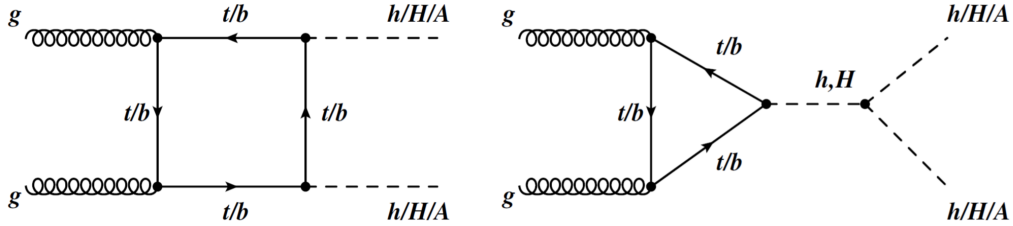
Figure 2.4: Generic diagrams contributing to pair production of MSSM Higgs bosons in gluon-gluon collisions (left) via box diagram and (right) via triangle diagrams.

2.4.1 MSSM pseudo scalar

Here we consider the production of CP even pseudo scalars via gluon fusion. The loop diagrams were evaluated using the tensor reduction explained in Passarino Veltman [22] for the Standard Model. We require several couplings including the trilinear Higgs

self couplings [Appendix B] which depends on β and the mixing angle α. MSSM
pseudo scalar production $gg \rightarrow A^0 A^0$ was considered first and then the pseudo scalar
decaying into a $b\bar{b}$ pair was evaluated. Fig 2.5 presents the calculated cross sections
for $gg \rightarrow A^0 A^0 + X$ for three selected $tan\,\beta$ values.
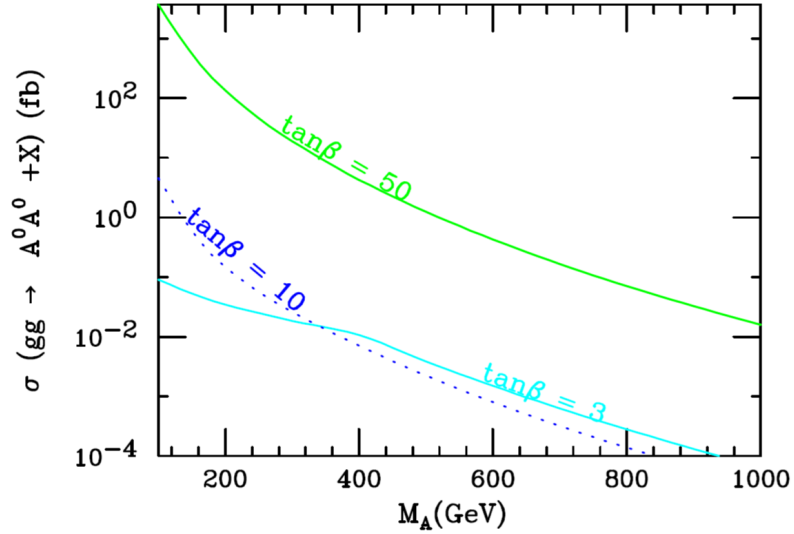
Figure 2.5: Leading order cross section for the production of pseudo scalars
via gluon fusion for three different $tan\,\beta$ values.

We first consider both pseudo scalars decaying into two pairs of b so that cross
sections were calculated for the process $gg \rightarrow A^0 A^0 \rightarrow b\bar{b}b\bar{b} + X$. Fig. 2.6 shows the
resulting cross section values after the pseudo scalar Higgs decay into b pairs, and the
values are calculated for $\sqrt{s} = 14\ TeV$ and integrated luminosity $\mathcal{L} = 30\ fb^{-1}$. The
same cuts, scales and pdfs were used here as explained for the Standard Model.

Next we considered the production of the MSSM pseudo scalar via gluon fusion
with one Higgs decaying into a pair of b quarks and the other Higgs decaying into
tau leptons followed by tau leptons with one tau decaying leptonically and the other

hadronically.
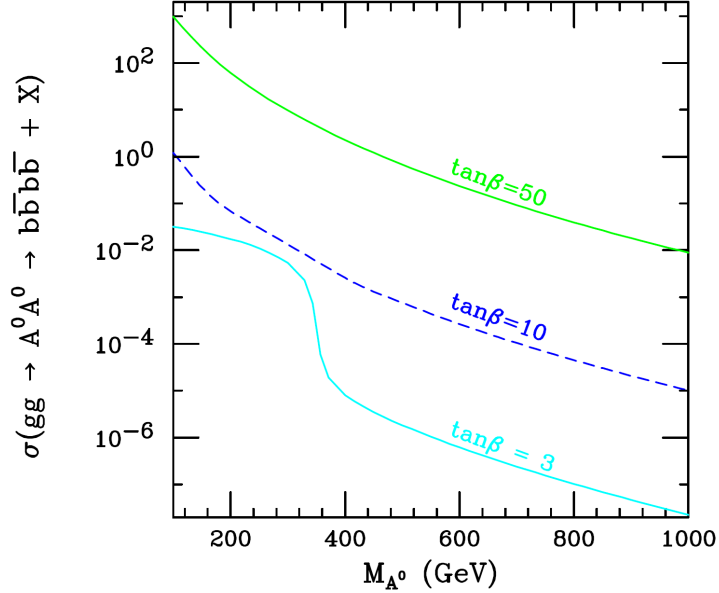
Figure 2.6: Leading Order cross section in (fb) for the process $gg \rightarrow A^0 A^0 \rightarrow b\bar{b}b\bar{b} + X$.

The LO cross sections calculated for $pp \rightarrow (A^0 \rightarrow b\bar{b})(A^0 \rightarrow \tau^+\tau^- \rightarrow lj_\tau + \not{E}_T)$ are presented in Fig. 2.7. Except the points discussed here, all other parameters, scales, cuts and methods are the same as explained in previous sections.

2.4.2 MSSM Light Higgs

CP even light Higgs in the MSSM is considered to be almost identical to the Standard Model Higgs boson. Since the SM Higgs mass is a known parameter now, the parameter space for light Higgs can be limited to certain values. FeynHiggs 2.9.1[26] was used here in terms of calculating the light Higgs masses and related parameters. Fig.2.8 shows the light Higgs mass in the parameter space of $tan\beta$ and M_A. The three curves drawn in the Fig. 2.8 which are for $M_h = 125.5$ GeV which is the exact SM Higgs
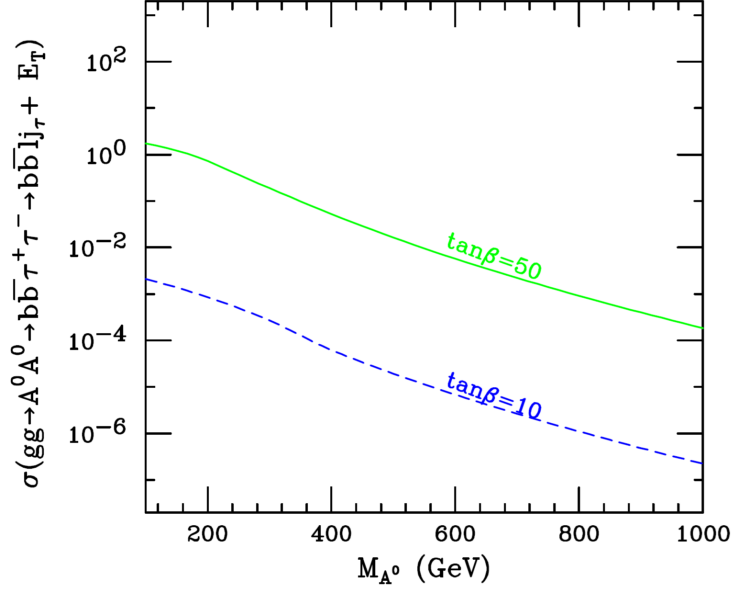
Figure 2.7: LO cross sections for the process $gg \rightarrow (A^0 \rightarrow b\bar{b})(A^0 \rightarrow \tau^+\tau^- \rightarrow lj\tau + \not{E}_T$ for two different $tan\,\beta$ values.

mass and other two for 122.5 GeV and 128.5 GeV. FeynHiggs requires a few variables to be inputed in text file "var.in", and this program calculates the masses of MSSM Higgs bosons and other important observables such as mixing angles, branching ratios, couplings and many more. Two sets of input parameters were considered in this case, and the light Higgs masses and related parameters were calculated accordingly. Two cases we considered here were case (a) $Msusy = 1000\ GeV$, $X_t = 2000$ GeV and case (b) $Msusy = 2000$ GeV , $X_t = (\sqrt{6} * Msusy)$. The details of all parameters of the input text file for the FeynHiggs executable is given in the Appendix C. M_A (mass of pseudo scalar) and TB($tan\beta$) which are the free parameters of the MSSM were changed over the selected ranges of values. As can be seen from two plots for $M_A > 250$ GeV, $tan\,\beta$ remains almost at a constant value in the range between 3 to

21

14. So we limited our calculation for selected values of $tan\,\beta$. FeynHiggs uses input variables to calculate the masses, mixing angles, branching ratios, couplings, etc. for the MSSM Higgs bosons.
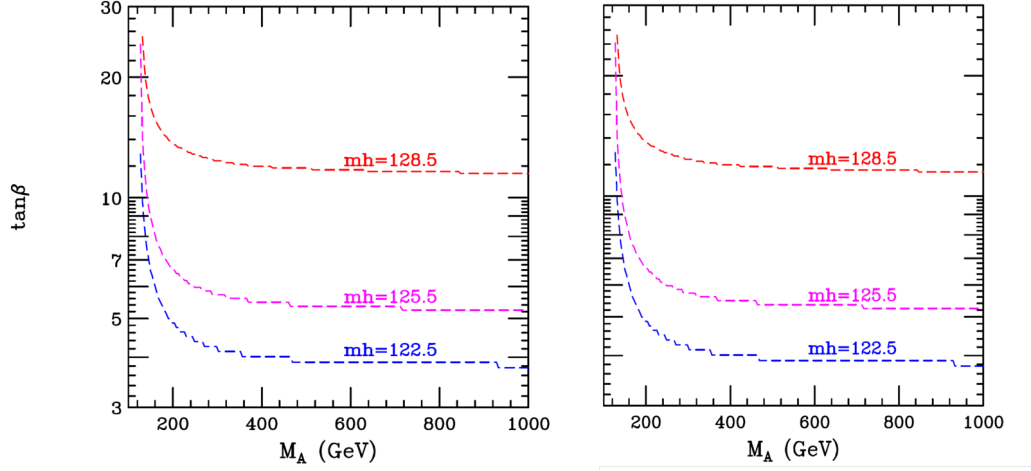
Figure 2.8: Change in light Higgs mass in the parameter space of $tan\,\beta$ vs MA. Left figure is for case(a) and right figure is for case(b) explained in the text.

The decay of Light Higgs to two pairs of $b\bar{b}$ was considered, and the cross section was calculated for the process $pp \rightarrow h^0 h^0 \rightarrow b\bar{b}b\bar{b} + X$. Figure 2.9 shows the calculated cross sections(in fb) for the process for MA changing from 250 GeV to $1000 GeV$ and for three most appropriate $tan\,\beta$ values. Pdfs and cuts used here were the same as we explained in previous sections. The two plots given in the Fig. 2.9 explain the two cases explained above according to the variables input to the FeynHiggs to produce light Higgs mass and other related parameters.

For the second step, a process where one light Higgs decay into $b\bar{b}$, and the other decays into $\tau^+\tau^-$ with the τ further decaying was considered. Cross sections calculated
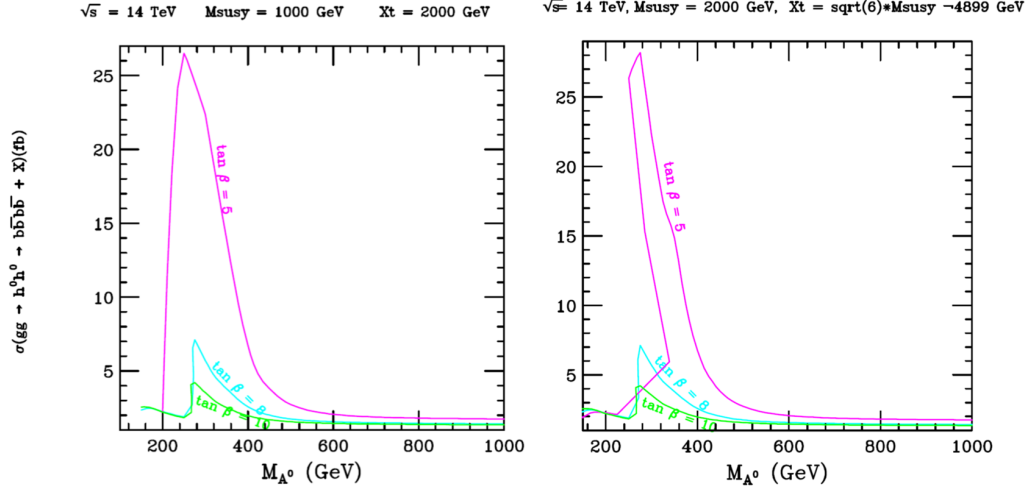
Figure 2.9: Leading order cross sections for the process $gg \to h^0 h^0 \to b\bar{b}b\bar{b}+X$, where h^0 is light Higgs. Left figure is for the light Higgs generated for $M_{susy} = 1000\ GeV$, $X_t = 2000\ Gev$ and right figure is for the light Higgs generated for $M_{susy} = 2000\ GeV$, $X_t = (\sqrt{6} * M_{susy})$.

for this process $gg \to (h^0 \to b\bar{b})(h^0 \to \tau^+\tau^- \to lj_\tau + \not{E}_T)$ are graphed as a function of M_A in Fig. 2.10.

2.4.3 MSSM Heavy Higgs

Fig. 2.11 shows the mass of the heavy Higgs(M_{H^0}) vs M_A and is drawn for several $tan\ \beta$ values. As can be seen from the figure for $M_A \geq 200$ GeV and higher $tan\ \beta$ values, the heavy Higgs is almost degenerate with the behavior of the pseudo scalar. Even with the difference of couplings heavy Higgs should reproduce the cross sections calculated for pseudo scalar.

This chapter covered the production cross sections of the signal using the mentioned processes. A detailed analysis of these values along with the backgrounds associated
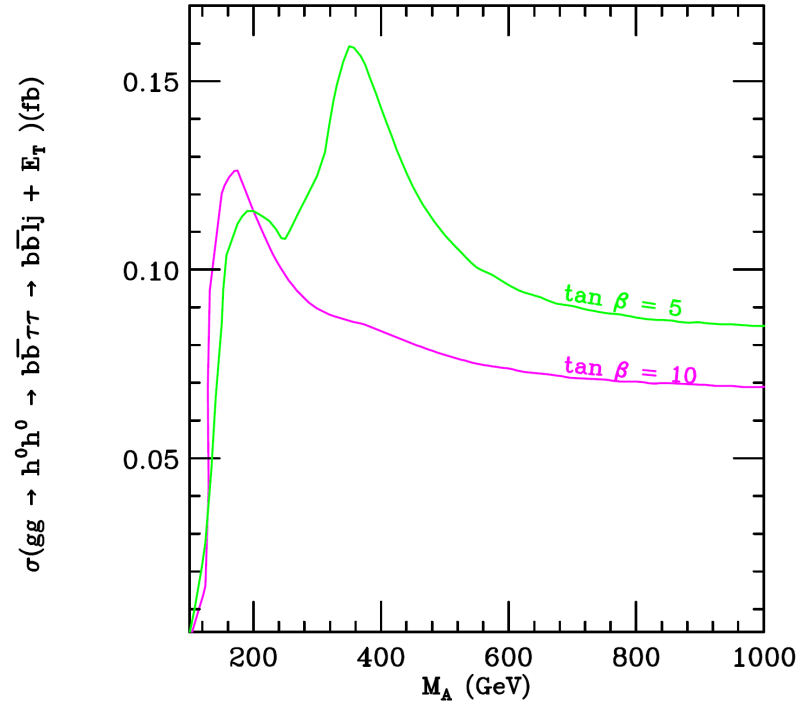
Figure 2.10: Leading order cross sections for the process $gg \to (h^0 \to b\bar{b})(h^0 \to \tau^+\tau^- \to lj_\tau + \not{E}_T)$ for $M_{susy} = 1000 GeV$.

with them, will be discussed in Chapter 4 with the significant improvements for the 4b final state.
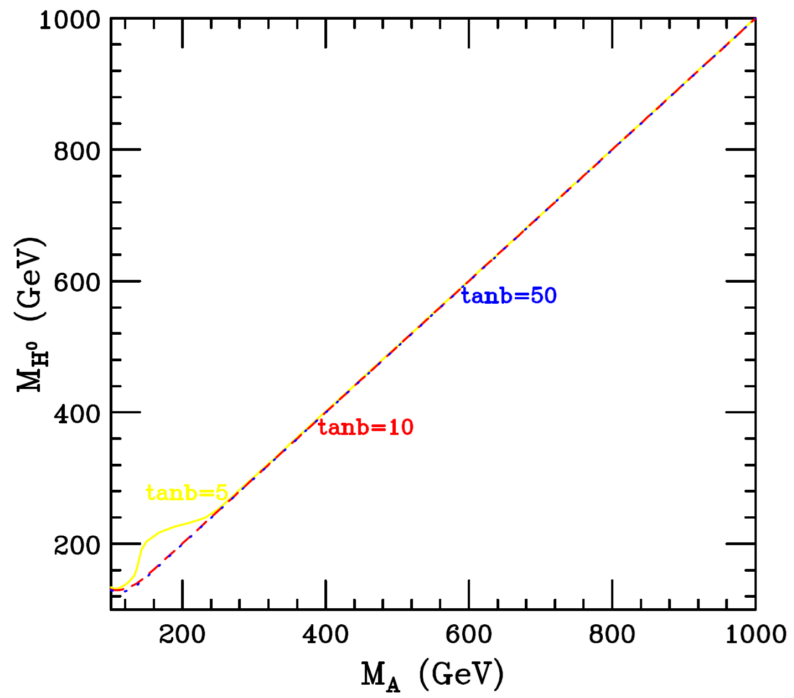
Figure 2.11: Mass of heavy Higgs bosons at one loop correction, different colors correspond to different $tan\ \beta$ values.

Chapter 3

Higgs Production Through b Quark Fusion

In the MSSM, the neutral Higgs bosons are dominantly produced from bottom quark fusion. The Higgs coupling to the fermion depends on m_f/v term, where m_f is the mass of the fermion and v is the vacuum expectation value. Since $m_b \approx 4.7\ GeV$, this Yukawa coupling is weak, which leads to a very small cross section for associated production of Higgs bosons. With the introduction of more than one Higgs doublet in the MSSM, this Yukawa coupling can be enhanced by a factor of $1/cos\beta$, and therefore the cross section associated with bottom quarks can be enhanced by choosing a higher value of $tan\,\beta$. Therefore, for $tan\,\beta > 7$, bottom quark fusion is the dominant process to produce neutral Higgs bosons in the MSSM. In the literature, a number of studies have been carried out about the Higgs production from b quarks. Reference [27] presents a NLO calculation for the total cross section of Higgs pair production via bottom quark fusion ($b\bar{b} \to hh$) at LHC in the SM. A study of supersymmetric QCD corrections for the Higgs pair production via bottom quark has been presented in [28]. References [29] [30] [31] are a few more studies done on heavy quark fusion and references [32], [33] discuss the Higgs boson production in association with single bottom quark. In this study, we focused on the production of neutral Higgs bosons with a bottom quark pair(b and $\bar{b}$) followed by Higgs decay into a pair of bottom quarks. We also consider the Higgs decay channel of $b\bar{b}\tau^+\tau^-$ with τ decay into leptons, jets and some missing energy. These processes are especially interesting because they

consist of diagrams with trilinear Higgs coupling which leads to measuring it in the future runs at LHC. Production cross sections of neutral Higgs bosons in MSSM will be mainly discussed in this chapter and numerical results will be presented for MSSM.

3.1 Leading order cross section for $b\bar{b} \to \phi^0\phi^0 + X$ in MSSM

Fig. 3.1 shows the tree level Feynman diagrams which contributes for $b\bar{b} \to \phi^0\phi^0$ in MSSM.
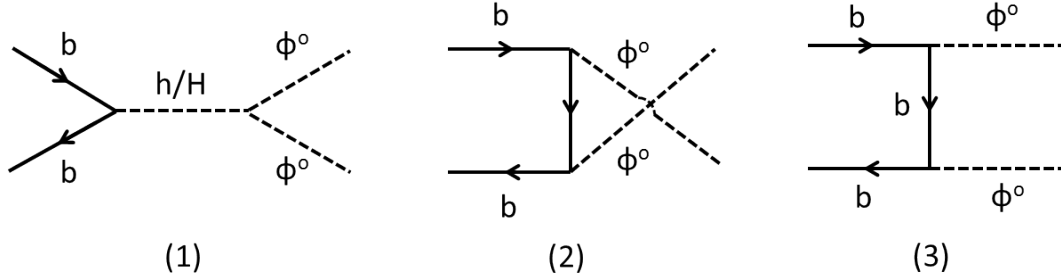
Figure 3.1: The lowest order Feynman diagrams for the production of Higgs boson pair in MSSM from b quark fusion, $\phi^0 = h^0, H^0, A^0$.

For the given Feynman diagrams in the Fig. 3.1, with the initial and final momenta set to be, $b(p_1)\bar{b}(p_2) \to \phi^0(p_3)\phi^0(p_4)$, and $p_1 + p_2 = p_3 + p_4$, the cross section can be simply written as,

$$\sigma_{LO} = \int dx_1 dx_2 [b(x_1)\bar{b}(x_2) + \bar{b}(x_1)b(x_2)] \times \hat{\sigma}_{LO}(b\bar{b} \to \phi^0\phi^0) \qquad (3.1)$$

where $b(x)$ and $\bar{b}(x)$ are the LO parton distribution functions for the bottom quarks and $\hat{\sigma}_{LO}$ is the parton level cross section for $(b\bar{b} \to \phi^0\phi^0)$. The Parton level differential

cross section over the two body phase space can be written as,

$$\frac{d\sigma}{d\Omega} = \left(\frac{\hbar c}{8\pi}\right)^2 \frac{S\,|M|^2}{(E_1 + E_2)^2} \frac{|p_f|}{|p_i|} \tag{3.2}$$

Here, $|p_f|$ is the magnitude of either outgoing momentum and $|p_i|$ is the magnitude of either incoming momentum. S is a product of statistical factors. M is the average amplitude for the process and ,

$$|M|^2 = \left(\frac{1}{3}\frac{1}{3}\right)\left(\frac{1}{2}\frac{1}{2}\right)\sum_{spin,\ color}|M_0|^2$$

The amplitude for each diagram can be written in the following form.

$$M_s^0 = \left(\frac{ig_{hbb}g_{h\phi\phi}}{s - M_h{}^2 + iM_h\Gamma_h} + \frac{ig_{Hbb}g_{H\phi\phi}}{s - M_H{}^2 + iM_H\Gamma_H}\right)\left(\overline{v}(p_2)P_L u(p_1) + \overline{v}(p_2)P_R u(p_1)\right)\delta_{\alpha\beta}$$

$$M_t^0 = \frac{g_{\phi bb}^2}{t}\left(\overline{v}(p_2)\not{p_3}P_L u(p_1) + \overline{v}(p_2)\not{p_3}P_R u(p_1)\right)\delta_{\alpha\beta}$$

$$M_u^0 = -\frac{g_{\phi bb}^2}{u}\left(\overline{v}(p_2)\not{p_3}P_L u(p_1) + \overline{v}(p_2)\not{p_3}P_R u(p_1)\right)\delta_{\alpha\beta}$$

where α, β are color indices for initial b and $\overline{b}$, $P_{R,L} = (1 \pm \gamma_5)/2$ and s, t, u are Mandelstam variables defined as

$$s = (p_1 + p_2)^2$$

$$t = (p_1 - p_3)^2$$

$$u = (p_2 - p_3)^2$$

28

The $g_{\phi bb}$ denotes the Yukawa couplings and $g_{h\phi\phi}$ and $g_{H\phi\phi}$ are trilinear Higgs couplings given in Appendices A and B. Γ_h is the decay width of the Higgs boson. The total amplitude was calculated by squaring the corresponding spin and color averaged matrix elements including interference terms.

3.2 Calculation Tools

The cross section is calculated using the NWA for $pp \rightarrow \phi^0\phi^0 \rightarrow b\bar{b}b\bar{b} + X$ via $b\bar{b} \rightarrow \phi^0\phi^0$ where, $\phi^0 = h^0, A^0, H^0$ for MSSM. Transition amplitudes were calculated both analytically and by using MadGraph for comparison purposes. The masses of the quarks for coupling terms were chosen to be the NLO running masses which are calculated at the pole masses of $m_t = 173.1$ GeV and $m_b = 4.7$ GeV. The renormalization scale is set to be $\mu_R = m_\phi/2$ for the calculation of strong coupling and running masses. Finally we simulate the pp collisions by applying the parton distribution functions of MSTW2008 with the factorization scale $\mu_F = m_\phi/2$. The light Higgs and Heavy Higgs masses and mixing angles were calculated using FeynHiggs for different SUSY parameters as discussed in Chapter 2. All other masses, couplings, cuts and other constants were calculated the same way as discussed in Chapter 2 for the gluon fusion processes.

3.3 Numerical Results

3.3.1 Standard Model

In the SM, bottom quark fusion can produce Higgs pairs at a small rate compared to gluon fusion. However, here we evaluate the leading order cross section for the production of Standard Model Higgs pair as an initiation for the extended models. Leading order cross sections evaluated for Higgs pair production from $b\bar{b}$ in the SM are given in Table 3.1. The cross section for the complete processes after the decay of the Higgs is also included in this table. The cuts explained in the gluon fusion were used here for the final state particles.

	$M_h = 123$ GeV	$M_h = 126$ GeV	$M_h = 129$ GeV
$\sigma(b\bar{b} \to hh)$	8.96×10^{-2}	8.55×10^{-2}	8.16×10^{-2}
$\sigma(b\bar{b} \to hh \to b\bar{b}b\bar{b} + X)$	3.70×10^{-2}	3.06×10^{-2}	2.47×10^{-2}

Table 3.1: Leading order cross section in fb for Standard Model Higgs pair production via b quark fusion. Cross sections for the complete processes after Higgs decay are also given.

3.3.2 Higgs pair production from b quark fusion in MSSM

Higgs pair production via bottom quark fusion in the MSSM is more interesting due to enhanced Yukawa couplings in two Higgs doublet Models. These enhanced Higgs pair production rates are significant in exploring trilinear Higgs coupling at

the LHC. Hence the calculation of production cross sections through b quark at LHC is motivated by MSSM. The cross sections for $pp \rightarrow \phi^0\phi^0 \rightarrow b\bar{b}b\bar{b} + X$ and $pp \rightarrow \phi^0\phi^0 \rightarrow b\bar{b}\tau^+\tau^- \rightarrow b\bar{b}l_\tau j_\tau + X$ were evaluated at $\sqrt{s} = 14$ TeV for $\phi^0 = A^0, h^0, H^0$, the three neutral Higgs bosons in MSSM. Fig. 3.2 shows the production cross sections of the pseudo scalar as a function of free parameter M_A for two $tan\,\beta$ values. Production cross sections in the MSSM via $b\bar{b}$ are higher compared to the cross sections in the SM Higgs production with the introduction of $tan\,\beta$. The values increase significantly with the increasing value of $tan\,\beta$.
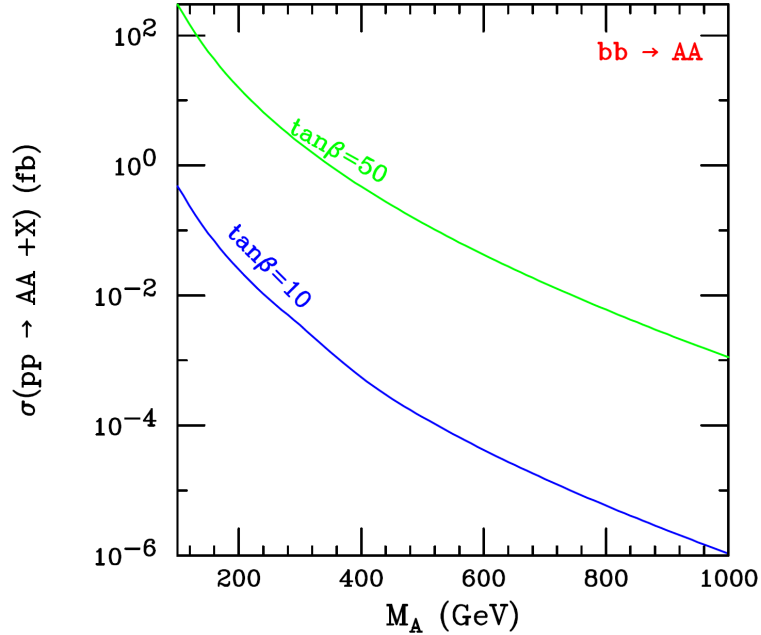
Figure 3.2: Leading order cross sections for the pair production of pseudo scalars from bottom quark fusion versus mass M_A(solid line). Green represents $tan\,\beta = 50$ and blue represents $tan\,\beta = 10$.

Pseudoscalars produced from $b\bar{b}$ collisions that decay into $b\bar{b}$ was considered and
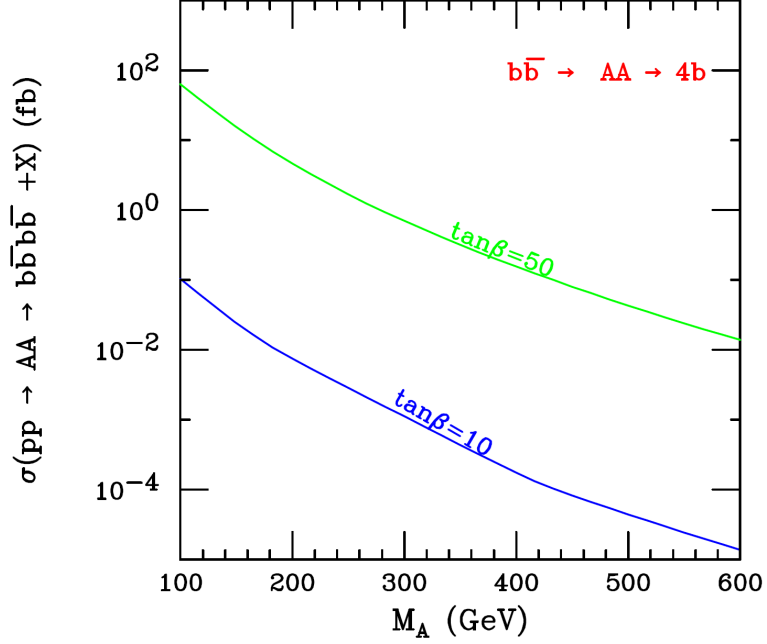
Figure 3.3: LO cross sections evaluated for $b\bar{b}b\bar{b}$ final state via pseudo scalars from b quark fusion(solid line). Green represents $tan\,\beta = 50$ and blue represents $tan\,\beta = 10$.

$\sigma(pp \to A^0A^0 \to b\bar{b}b\bar{b} + X)$ vs mass for the pseudo scalar was plotted in Fig. 3.3. The cross sections from $b\bar{b}$ are very close to the cross sections evaluated from gluon fusion even with smaller PDFs for b quark compared to gluon PDFs. Fig. 3.4 presents the leading order cross sections for the $b\bar{b}lj_{\tau}$ final state via pseudoscalars produced from b quark fusion. Cross sections are smaller compared to 4b final state though the significance of background vs signal will be better due to a cleaner background in this case.

As discussed in Chapter 2, since the MSSM light Higgs should have a mass close to the SM Higgs, setting $tan\beta$ to very high values is not meaningful in this case. Cross
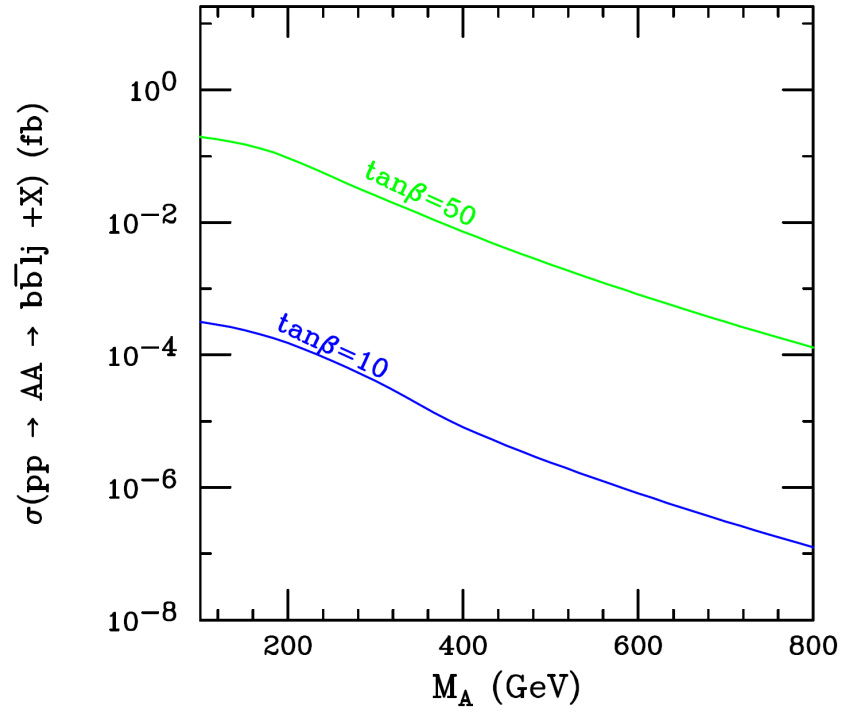
Figure 3.4: Leading order cross section for the production of the pseudoscalar(A^0) followed by $A^0 A^0 \to b\bar{b}\tau^+\tau^- \to b\bar{b}lj_\tau + E\!\!\!/_T$.

sections were evaluated for $tan\beta = 5$ and $tan\beta = 10$ for the light Higgs production via

$b\bar{b}$ fusion with the Higgs decaying into $b\bar{b}$. Leading order cross sections for production of

light Higgs bosons were evaluated for $4b$ and $bb\tau\tau$ channels. The results are presented

in the figures 3.5 and 3.6 respectively.
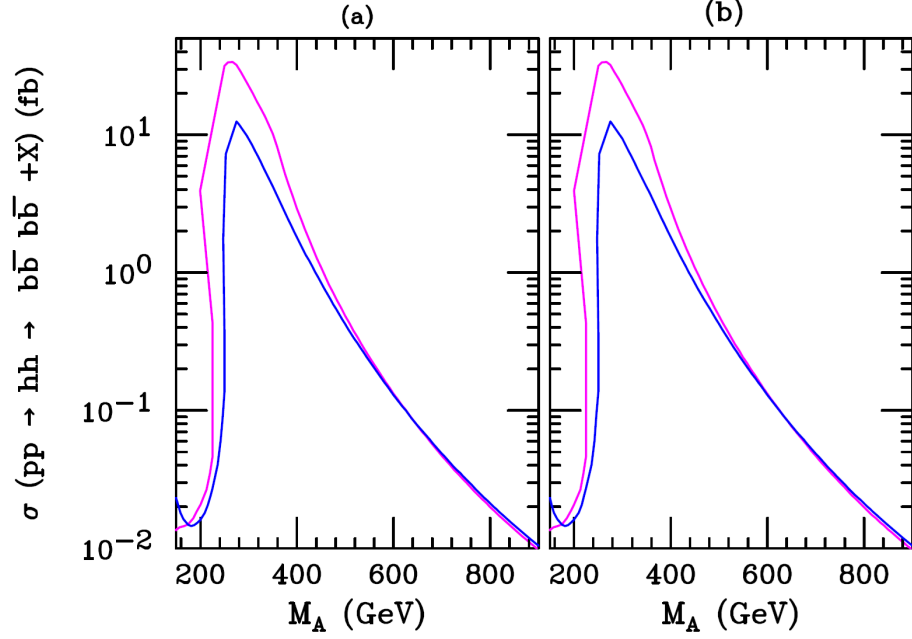
Figure 3.5: LO cross sections for $pp \rightarrow \phi\phi \rightarrow b\bar{b}b\bar{b} + X$ via b quark fusion.

ϕ is the MSSM light Higgs. Magenta represents $tan\ \beta = 5$ and blue

represents $tan\ \beta = 10$ b quark fusion. (a) For light Higgs produced with

$Msusy = 1000\ GeV$, $X_t = 2000\ GeV$ (b) For light Higgs produced with

$Msusy = 2000\ GeV$, $X_t = (\sqrt{6} * MSusy)$.
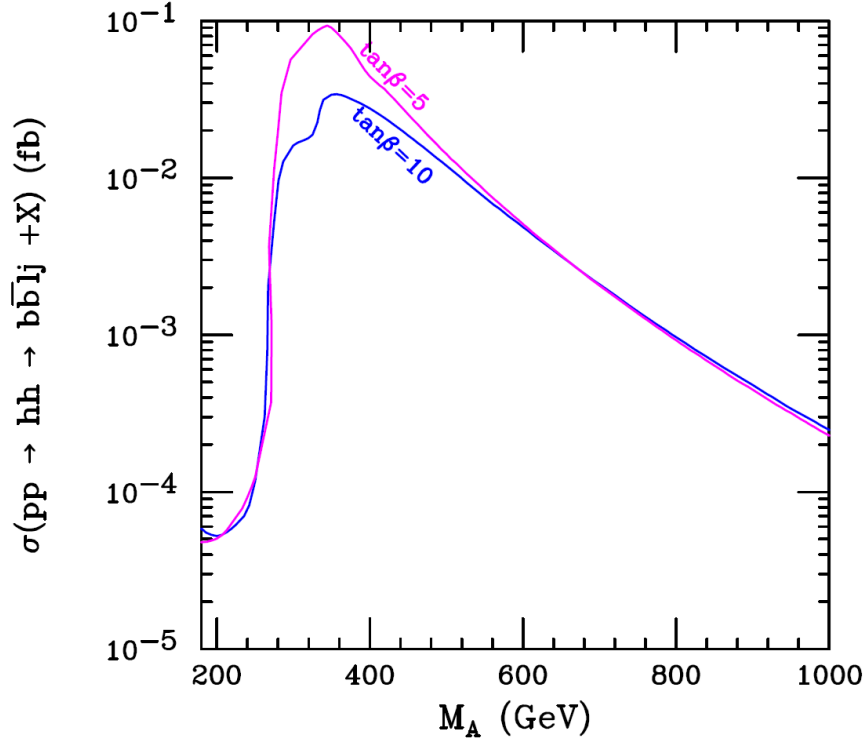
Figure 3.6: LO cross section for the process $pp \rightarrow \phi\phi \rightarrow b\bar{b}\tau^+\tau^- \rightarrow b\bar{b}lj_\tau + \not{E}_T + X$ via $b\bar{b}$ fusion as a function of M_A. MSSM light Higgs masses were evaluated for $Msusy = 2000$ GeV and $X_t = \sqrt{6} \times Msusy$. Magenta represent $tan\,\beta = 5$, blue represent $tan\,\beta = 10$.

Chapter 4

Analysis of Backgrounds for $(b\bar{b})(b\bar{b})$ final state

The dominant background processes associated with two Higgs production at the LHC, discussed in previous two chapters, are analyzed here. We discuss the relevant background processes coupled with $pp \to b\bar{b}b\bar{b}$ via gluon fusion for the SM and through b quark fusion for the MSSM. The Standard Model Higgs boson pair production with a $b\bar{b}b\bar{b}$ final state has been studied in [34] recently, and they discuss how to reduce large backgrounds through BDRS[35] approach.

However, with the highest branching ratio of 60% for $b\bar{b}$ channel in the SM, the highest cross sections at LHC result from gluon fusion with 4b final state. This process has not been of interest due to the large QCD backgrounds coupled to this process. However, we discuss the dominant tree level background events for the 4b final state resulting from parton collisions at the LHC. We try to reduce backgrounds by introducing a special mass cut and the reordering method explained in Chapter 2. This way we can increase the $S/\sqrt{B}$ ratio significantly and study the possibility of using this signal to measure trilinear Higgs couplings at the LHC. The relevant basic tree level processes considered here are,

1. $pp \to b\bar{b}b\bar{b}/h$

2. $pp \to b\bar{b}c\bar{c}/h$

3. $pp \to b\bar{b}jj/h$ where $j = u, d, s, g$

4.1 Calculation Tools

Cross sections were calculated for an LHC center of mass energy $\sqrt{s} = 14\ TeV$. Both renormalization and factorization scales were set to $\sqrt{\hat{s}}$, and MSTW2008 pdf were used here. The transition matrix elements were generated using a standalone version of MadGraph[36], and the cross sections were evaluated by integrating over the phase space using a FORTRAN program. In this study the tagging efficiency for b jet is set as $\epsilon_b = 60\%$ for $\mathcal{L} = 30\,fb^{-1}$ and $\epsilon_b = 50\%$ for $\mathcal{L} = 300\,fb^{-1}$ and $3000\,fb^{-1}$. Mistagging probabilities of fake jets as b jet are set to $\epsilon_c = 10\%$ and $\epsilon_j = 1\%$. As discussed in Chapter 2, several cuts were applied for the background namely, $P_T(b_i) > 30\ GeV$, $\eta(b_i) < 2.5$ and $\Delta_{bb} \geq 0.4$ where $i = 1, 2, 3, 4$ denotes final state b jets. These basic cuts could not improve the signal to background ratio significantly. With the introduction of special reordering and mass cuts(explained in chapter 2) for $M_{b_1 b_2}$ and $M_{b_3 b_4}$, we could remove 90% of the background while saving 80% of the signal. Fig. 4.1 is the mass distribution for the major background process which is $pp \rightarrow b\bar{b}b\bar{b}/h$ in the 4b final state. Invariant masses for each pair are evaluated after reordering so that M_{12} is the pair which has maximum $|xmbb - M_A|$ where $xmbb$ is the invariant mass between relevant b jets. K factors for Higgs pair production at each energy were calculated using the formula given in [20]. A K-factor of 1.5 was applied to the QCD$(b\bar{b})(b\bar{b})$ background.
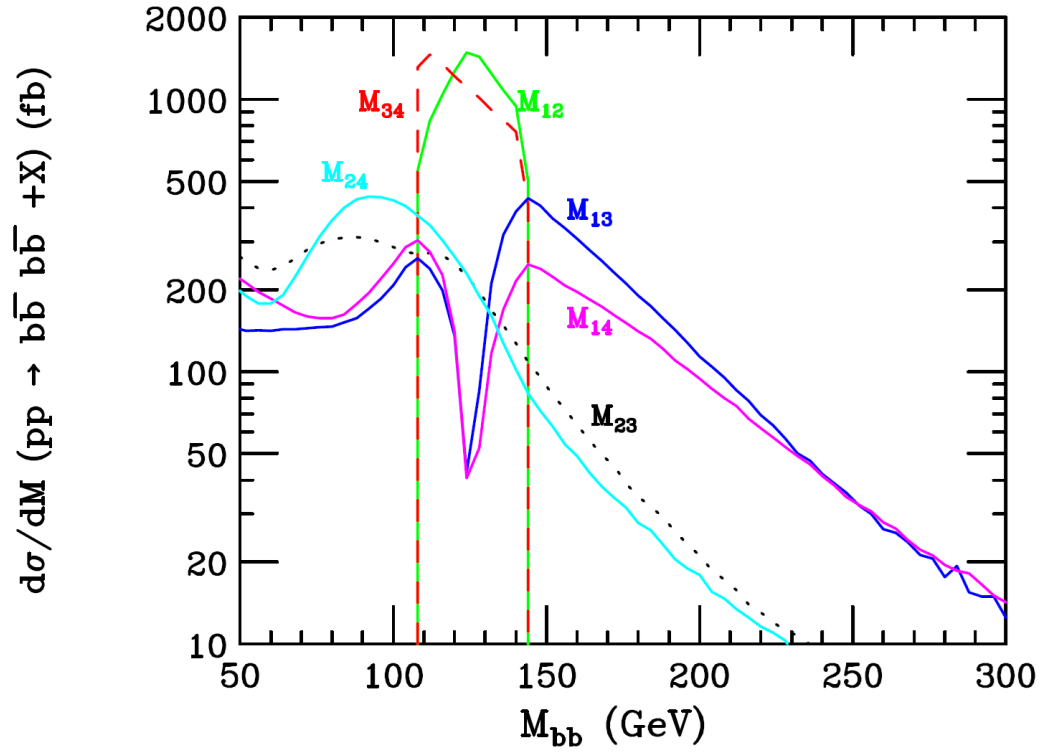
Figure 4.1: The mass distribution of final state b jets for the dominant background process $pp \rightarrow b\bar{b}b\bar{b}/h + X$, with the special mass reordering explained in the text.

Energy (TeV)	$pp \rightarrow hh \rightarrow 4b$	$pp \rightarrow b\bar{b}b\bar{b}/h$	$pp \rightarrow b\bar{b}c\bar{c}/h$	$pp \rightarrow b\bar{b}jj/h$	Total BG
13	4.57	6.80×10^3	1.44×10^4	1.16×10^6	1.56×10^3
14	5.40	7.90×10^3	1.66×10^4	1.35×10^6	1.81×10^3
33	2.90×10^1	3.61×10^4	7.61×10^4	5.92×10^6	8.27×10^3
60	7.77×10^1	9.23×10^4	1.95×10^5	1.52×10^7	2.10×10^4
100	1.68×10^2	1.90×10^5	4.13×10^5	3.18×10^7	4.45×10^4

Table 4.1: Cross sections (in fb) for SM Higgs production via gluon fusion for $\mathcal{L} = 30fb^{-1}$. In the 6th column, Total BG is the background value after considering relevant tagging efficiencies and K-factors.

4.2 Standard Model through Gluon Fusion

Table 4.1 shows the cross sections obtained in this study for SM Higgs production (with Higgs decaying into 4 b jets) via gluon fusion along with the dominant tree level backgrounds for several energies. The 3rd 4th and 5th columns of this table give the values of three major backgrounds listed earlier. Tagging efficiencies or K-factors are not counted towards these values. For the third background(5th column) listed in this table, only $pp \rightarrow b\bar{b}gg$ and $pp \rightarrow b\bar{b}ug$ were considered since the contribution from all other combinations of jets is negligible. The 6th column gives the total contribution of all dominant background processes along with tagging efficiencies and QCD corrections.

Table 4.2 presents the calculated significance values for different luminosities vs

energies. The significance of the signal vs background can be defined as,

$$N_{SS} = \frac{N_s}{\sqrt{N_b}}$$

where $N_s = \mathcal{L} \times \sigma_s$ is the number of signal events and $N_b = \mathcal{L} \times \sigma_b$ is the number of

events for background.

Luminosity $\sqrt{s}$	$\mathcal{L} = 30\,fb^{-1}$	$\mathcal{L} = 300\,fb^{-1}$	$\mathcal{L} = 3000\ fb^{-1}$
$13\,TeV$	0.634	2.01	6.34
$14\,TeV$	0.695	2.19	6.94
$33\,TeV$	1.74	5.51	17.5
$60\,TeV$	2.92	9.26	29.3
$100\,TeV$	4.36	13.8	43.7

Table 4.2: Calculated N_{ss} values for different integrated luminosities and

energies for the SM Higgs production via gluon fusion.

As can be seen from the Table 4.2, we could improve $S/\sqrt{B}$ significantly for the $4b$

final state with the introduction of new mass cut. For $\sqrt{s} = 14\ TeV$, $N_{ss} = 2.19(6.94)$

with 14(137) signal events for the integrated luminosities of 300(3000) fb^{-1} which

shows that there is a possibility of measuring trilinear Higgs couplings at the LHC in

the future.

$\sqrt{s}$	N_s	N_s/N_b	N_{ss}
14 TeV	137	0.003	6.94

Table 4.3: Calculated $N_s, N_s/N_b, N_{ss}$ values for integrated luminosity of $3000\ fb^{-1}$ and for $\sqrt{s} = 14$ TeV for the SM Higgs production via gluon fusion.

4.3   MSSM through b Quark Fusion

Here we discuss the backgrounds associated with MSSM Higgs production followed by Higgs decay into two pairs of b quarks. The processes are the same as we discussed for the SM gluon fusion though we have two free parameters here M_A and $tan\beta$. As could be seen from chapter 3, b quark fusion is more important for high values of $tan\ \beta$ and therefore we chose $tan\ \beta$ to be 30, 50, and cross sections were calculated for several values of M_A. For the signal $bb \to \phi\phi \to b\bar{b}b\bar{b} + X$ was considered, and for the chosen value of $tan\beta$, the contribution from the pseudo scalar and heavy Higgs were counted. For the evaluation of background processes, both renormalization and factorization scales were set to $\sqrt{\hat{s}}$. Table 4.4 presents the backgrounds and $S/\sqrt{B}$, calculated for low luminosity ($\mathcal{L} = 30\ fb^{-1}$) with transverse momentum $P_T > 20\ GeV$ for all b jets and tagging efficiency of 60%. Fig. 4.5 presents the same information for high luminosity $\mathcal{L} = 300\ (3000)\ fb^{-1}$ and $P_T > 30\ GeV$ and $\epsilon_b = 50\%$. All other cuts are the same as explained before and $\sqrt{s} = 14$ TeV.

M_A	200 GeV	400 GeV	800 GeV
$\sigma_s(tan\,\beta = 30)$	1.1	3.8×10^{-2}	4.9×10^{-4}
$\sigma_s(tan\,\beta = 50)$	8.54	3.04×10^{-1}	3.86×10^{-3}
$\sigma_b(pp \to b\bar{b}b\bar{b}/h)$	5.93×10^3	3.26×10^2	6.38
$\sigma_b(pp \to b\bar{b}c\bar{c}/h)$	3.86×10^5	4.09×10^4	2.33×10^3
$\sigma_b(pp \to b\bar{b}jj/h)$	3.29×10^7	3.48×10^6	2.09×10^5
$\sigma_b(total)$	7.6×10^3	7.47×10^2	4.1×10^1
$N_s(tan\,\beta = 30)$	36	1	0
$N_s(tan\,\beta = 50)$	256	9	0
$N_s/N_b\ (tan\,\beta = 30)$	1.58×10^{-4}	5.08×10^{-5}	1.21×10^{-5}
$N_s/N_b\ (tan\,\beta = 50)$	1.12×10^{-3}	4.06×10^{-5}	9.45×10^{-5}
$N_{ss}(tan\,\beta = 30)$	0.08	0.008	0.0004
$N_{ss}(tan\,\beta = 50)$	0.54	0.06	0.003

Table 4.4: MSSM Higgs production via b quark fusion $b\bar{b} \to \phi^0\phi^0 \to b\bar{b}b\bar{b} + X$ at LHC at $\sqrt{s} = 14\,TeV$ for $\mathcal{L} = 30fb^{-1}$.

M_A	200 GeV	400 GeV	800 GeV
$\sigma_s(\tan\beta = 30)$	1.1	3.8×10^{-2}	4.9×10^{-4}
$\sigma_s(\tan\beta = 50)$	8.54	3.04×10^{-1}	3.86×10^{-3}
$\sigma_b(pp \rightarrow b\bar{b}b\bar{b}/h)$	3.01×10^3	2.6×10^2	6.35
$\sigma_b(pp \rightarrow b\bar{b}c\bar{c}/h))$	2.05×10^5	3.23×10^4	2.27×10^3
$\sigma_b(pp \rightarrow b\bar{b}j\bar{j}/h)$	1.71×10^7	2.74×10^6	1.99×10^5
$\sigma_b(total)$	2.65×10^3	3.99×10^2	2.72×10^1
$N_s(\tan\beta = 30)$	300	11	0.2
$N_s(\tan\beta = 50)$	2562	9	1
$N_s/N_b \ (\tan\beta = 30)$	4×10^{-4}	9.5×10^{-5}	1.8×10^{-6}
$N_s/N_b \ (\tan\beta = 50)$	3.0×10^{-3}	7.6×10^{-4}	1.4×10^{-5}
$N_{ss}(\tan\beta = 30)$	0.4(1.17)	0.03(0.10)	$1.6 \times 10^{-3}(5.2 \times 10^{-3})$
$N_{ss}(\tan\beta = 50)$	2.87(9.07)	0.263(0.83)	$1.3 \times 10^{-2}(4.0 \times 10^{-2})$

Table 4.5: MSSM Higgs production via b quark fusion $b\bar{b} \rightarrow \phi^0\phi^0 \rightarrow b\bar{b}b\bar{b} + X$ at $\sqrt{s} = 14\,TeV$ for $\mathcal{L} = 300(3000)\,fb^{-1}$. All cross section values are in fb.

Chapter 5

Analysis of Backgrounds for $b\bar{b}\tau^+\tau^-$ final state

The dominant background processes coupled with $pp \to b\bar{b}\tau^+\tau^- \to b\bar{b}lj_\tau + \not{E}_T$ via gluon fusion for the SM and through b quark fusion and gluon fusion for the MSSM are studied, and results are presented in this chapter. The neutral Higgs boson decays to $\tau^+\tau^-$ with a branching ratio of about 10% which is much smaller than that of $\phi \to b\bar{b}$ which is 60%. However, this process is considered to be more promising than the $4b$ final state because the backgrounds can be swept out by adjusting different cuts for the invariant mass of τ leptons which also will be discussed in this chapter. In this study we consider the largest decay mode of $\tau^+\tau^-$which is where one decays to leptons and other to a tau jet with $Br(\tau \to e/\mu) = 35.2\%$ and $Br(\tau \to \pi/\rho/a_1) = 54.8\%$. The dominant tree level processes we consider here are listed below.

1. $pp \to b\bar{b}\tau^+\tau^- \to b\bar{b}lj_\tau + X$

2. $pp \to c\bar{c}\tau^+\tau^- \to q\bar{q}lj_\tau + X$

3. $pp \to t\bar{t} \to bW^+\bar{b}W^- \to b\bar{b}\tau^+\tau^- \to b\bar{b}lj_\tau + X$

4. $pp \to t\bar{t} \to bW^+\bar{b}W^- \to b\bar{b}l^\pm\tau^\pm \to b\bar{b}lj_\tau + X$

5. $pp \to t\bar{t} \to bW^+\bar{b}W^- \to b\bar{b}ljj + X$

6. $pp \to tW^\pm \to bW^\pm\bar{b}W^\pm \to bljj + X$

$\mathcal{L}(fb^{-1})$	30	300
$P_T(GeV)$	$P_T(b,l,j_\tau) > 15, 20, 40$	$P_T(b,l,j_\tau) > 30, 20, 40$
η	$|\eta(b)|, |\eta(l)|, |\eta(j_\tau)| < 2.5$	$|\eta(b)|, |\eta(l)|, |\eta(j_\tau)| < 2.5$
ΔR	$\Delta R(l j_\tau) > 0.4$	$\Delta R(l j_\tau) > 0.4$
$\not{E}_T(GeV)$	$\not{E}_T > 40$	$\not{E}_T > 50$

Table 5.1: Basic cuts used for the production of the Higgs via $pp \rightarrow$ $b\bar{b}\tau^+\tau^- \rightarrow b\bar{b}l j_\tau + \not{E}_T$.

5.1 Calculation Tools

Cross sections were calculated for an LHC center of mass energy $\sqrt{s} = 14\,TeV$ and for low (30 fb^{-1}) and high (300 fb^{-1}) luminosities. Other than the tools explained, we have used slightly different cuts here for the $4b$ backgrounds than in previous chapters. They are listed in Table 5.1. In the processes including $t\bar{t}$, the events with extra b jets are vetoed if both b jets pass the selection cut which is $|M_{bb} - M_h| \leq 0.15 * M_h$ where M_{bb} is the invariant mass of $b\bar{b}$. Processes 5 and 6 have two light jets in the final state. We required that only one pass the cuts and then be mistagged as j_τ.

Though we apply the basic cuts mentioned in the table, backgrounds cannot be reduced significantly with only these basic cuts. Since there are no tau leptons in the final state of these processes, we have to reconstruct them from the kinematics of observable particles. As mentioned in Chapter 2, we use the Collinear Approximation and follow the procedure explained in [37] to reconstruct the momenta of tau leptons(P_{τ_1} ,P_{τ_2}). Based on the reconstructed momenta, the mass of the Higgs boson is the invariant

45

mass of the $\tau^+\tau^-$ pairs, $m_{\tau\tau} = (P_{\tau_1} + P_{\tau_2})^2$. By properly setting cuts on $m_{\tau\tau}$, we can remove most background events and enhance the discovery potential. Here we set $|m_{\tau\tau} - M_h| \leq 0.15 * M_h$ which reduced the cross section of the SM signal from $0.047\ fb$ to $0.065\ fb$ while all the background values can be reduced significantly. Table 5.2 presents the cross section values before and after the mass reconstruction from tau leptons. These values are calculated for SM Higgs $Mh = 125.5\ GeV$.

Process	With basic cuts	Cut on $m\tau\tau$
$pp \to b\bar{b}\tau^+\tau^- \to b\bar{b}lj_\tau + X$	2.03	0.216
$pp \to q\bar{q}\tau^+\tau^- \to q\bar{q}lj_\tau + X$	3.21	0.370
$pp \to t\bar{t} \to bW^+\bar{b}W^- \to b\bar{b}\tau^+\tau^- \to b\bar{b}lj + X$	17.2	0.469
$pp \to t\bar{t} \to bW^+\bar{b}W^- \to b\bar{b}l^\pm\tau^\pm \to b\bar{b}lj + X$	55.0	0.806
$pp \to t\bar{t} \to bW^+\bar{b}W^- \to b\bar{b}ljj + X$	977	9.66
$pp \to tW^\pm \to bW^\pm\bar{b}W^\pm \to bljj + X$	51.9	0.263

Table 5.2: Cross sections for the background processes listed after and before the cut apply on reconstructed mass from tau leptons. All the values are in fb and tagging efficiencies and K factors have not been included for these values.

The efficiency of tau jet triggering is 26%, and we assume that the charged leptons can be 100% correctly identified. The tagging probabilities of identifying fake jets as J_τ is $\epsilon_{u,d,c,s} = 1/400$ and $\epsilon_b = 1/700$. For the higher order corrections, results were multiplied with relevant K factors, and a K factor of 1.3 was used for first two

processes[38]; $K = 2$ for $t\bar{t}$ [39] [40], and $K = 1.5$ were included for the processes with tW [41].

5.2   Numerical Results

The dominant background processes explained above compared to the SM signal of $pp \to b\bar{b}\tau^+\tau^- \to b\bar{b}lj_\tau + \not{E}_T$ for different luminosities are presented in Tables 5.3 and 5.4. Same cuts and scales were applied for the signal too.

$\sigma_s(\mathcal{L} = 30(fb^{-1}))$	0.079
$\sigma_b(q\bar{q}\tau^+\tau^-)$	0.002
$\sigma_b(t\bar{t})$	0.26
$\sigma_b(tW)$	0.00035
N_s	2
N_s/N_b	0.3
N_{ss}	0.85

Table 5.3: Cross sections evaluated for the signal $gg \to b\bar{b}\tau^+\tau^- \to b\bar{b}lj_\tau + \not{E}_T$ in the SM along with dominant backgrounds for $\mathcal{L} = 30 \ fb^{-1}$ and $S/\sqrt{B}$ is presented in the last row.

Backgrounds were calculated for the MSSM neutral Higgs production via b quark fusion and were analyzed towards the signal discussed in Chapter 3. Again we consider two high $tan \ \beta$ values to see how we can increase the significance towards future measurements of trilinear Higgs coupling. Tables 5.5 and 5.7 give the cross section of

$\sigma_s(\mathcal{L} = 300 fb^{-1})$	0.0596
$\sigma_b(q\bar{q}\tau^+\tau^-)$	0.001
$\sigma_b(t\bar{t})$	0.177
$\sigma_b(tW)$	0.0002
N_s	18
N_s/N_b	0.33
N_{ss}	2.4(7.7)

Table 5.4: Cross sections evaluated for the signal $gg \to b\bar{b}\tau^+\tau^- \to b\bar{b}lj_\tau +$ $\not{E}_T$ in the SM along with dominant backgrounds for $\mathcal{L} = 300(3000)\ fb^{-1}$ and $S/\sqrt{B}$ is presented in the last row.

MSSM Higgs production via b quark fusion which is $bb \to b\bar{b}\tau^+\tau^- \to b\bar{b}lj_\tau + \not{E}_T$ along with relevant background processes. N_{ss} was calculated for different luminosities and for different $tan\ \beta$ values. In the Tables 5.5 and 5.7, q refers to quarks including b, and $\sigma_b(pp \to q\bar{q}\tau^+\tau^-/h)$ is the total background from process 1 and 2 listed above. Here we discuss the Higgs signal so that ϕ^0 has the contributions from all three A^0, h^0 and H^0. With the approximations for the SUSY parameters we set in FeynHiggs, the mass of the light Higgs maintains almost a constant value as $tan\ \beta$ increases. So for the most of the parameter space$(M_A, tan\ \beta)$, we considered the contributions from pseudoscalar and heavy Higgs.

Tables 5.6 and 5.8 present the results for the production of MSSM Higgs via gluon fusion and Higgs decaying into $b\bar{b}\tau^+\tau^- \to b\bar{b}lj_\tau + X$ for low and high luminosities

M_A	200 GeV	400 GeV	800 GeV
$\sigma_s(tan\,\beta = 30)$	2.44×10^{-2}	1.9×10^{-3}	3.4×10^{-5}
$\sigma_s(tan\,\beta = 50)$	1.89×10^{-1}	1.47×10^{-2}	2.63×10^{-4}
$\sigma_b(pp \to q\bar{q}\tau^+\tau^-/h)$	1.35×10^{-1}	5.87×10^{-2}	1.03×10^{-2}
$\sigma_b(pp \to t\bar{t} \to bW^+\bar{b}W^- \to b\bar{b}lj_\tau))$	3.29	1.77	4.1×10^{-1}
$\sigma_b(pp \to tW \to bW^{\pm}\bar{b}W^{\pm} \to bljj)$	6.79×10^{-4}	1.46×10^{-4}	1.25×10^{-5}
$\sigma_b(total)$	3.42	1.82	4.21×10^{-1}
$N_s(tan\,\beta = 30)$	1	0	0
$N_s(tan\,\beta = 50)$	6	0	0
$N_s/N_b(tan\,\beta = 30)$	7.1×10^{-3}	1.04×10^{-3}	8.08×10^{-5}
$N_s/N_b(tan\,\beta = 50)$	5.5×10^{-2}	8.08×10^{-3}	6.2×10^{-4}
$N_{ss}(tan\,\beta = 30)$	0.07	0.0077	0.00017
$N_{ss}(tan\,\beta = 50)$	0.56	0.06	0.002

Table 5.5: The MSSM Higgs production via b quark fusion $b\bar{b} \to \phi^0\phi^0 \to b\bar{b}\tau^+\tau^- \to b\bar{b}lj_\tau + X$ at $\sqrt{s} = 14\,TeV$ for $\mathcal{L} = 30fb^{-1}$. All cross section values are in fb.

M_A	σ_s	σ_b	N_s	N_s/N_b	N_{ss}
$200\ GeV$	3.85	3.42	116	1.13	11.42
$400\ GeV$	3.74×10^{-1}	1.82	11	0.2	1.52
$800\ GeV$	9.61×10^{-3}	0.421	0	0.0023	0.08

Table 5.6: The MSSM Higgs production via gluon fusion $gg \to \phi^0\phi^0 \to$ $b\bar{b}\tau^+\tau^- \to b\bar{b}lj_\tau + \not{E}_T$ at $\sqrt{s} = 14\,TeV$ for $\mathcal{L} = 30fb^{-1}$. These results are for $tan\ \beta = 50$, and all values are in fb.

respectively. These values are calculated for $tan\ \beta = 50$, and again the contributions from heavy Higgs are also considered.

M_A	200 GeV	400 GeV	800 GeV
$\sigma_s(tan\,\beta = 30)$	1.99×10^{-2}	1.81×10^{-3}	3.34×10^{-5}
$\sigma_s(tan\,\beta = 50)$	1.61×10^{-1}	1.51×10^{-2}	2.85×10^{-4}
$\sigma_b(pp \rightarrow q\bar{q}\tau^+\tau^-/h)$	7.7×10^{-2}	4.38×10^{-2}	9.14×10^{-3}
$\sigma_b(pp \rightarrow t\bar{t} \rightarrow bW^+\bar{b}W^- \rightarrow b\bar{b}lj_\tau))$	1.57	7.6×10^{-1}	1.91×-1
$\sigma_b(pp \rightarrow tW \rightarrow bW^{\pm}\bar{b}W^{\pm} \rightarrow bljj)$	4.4×10^{-4}	1.13×10^{-2}	1.08×10^{-5}
$\sigma_b(total)$	1.65	8.18×10^{-1}	2.0×10^{-2}
$N_s(tan\,\beta = 30)$	6	1	0
$N_s(tan\,\beta = 50)$	48	5	0
$N_s/N_b(tan\,\beta = 30)$	1.21×10^{-2}	2.21×10^{-3}	1.67×10^{-4}
$N_s/N_b(tan\,\beta = 50)$	9.7×10^{-2}	1.85×10^{-2}	1.42×10^{-3}
$N_{ss}(tan\,\beta = 30)$	0.268(0.848)	0.0347(0.11)	0.0013(0.004)
$N_{ss}(tan\,\beta = 50)$	2.16(6.84)	0.289(0.915)	0.011(0.035)

Table 5.7: MSSM Higgs production via b quark fusion $b\bar{b} \rightarrow \phi^0\phi^0 \rightarrow$ $b\bar{b}\tau^+\tau^- \rightarrow b\bar{b}lj_\tau + \not{E}_T$ at $\sqrt{s} = 14\,TeV$ for $\mathcal{L} = 300(3000)fb^{-1}$. All cross section values are in fb.

M_A	σ_s	σ_b	N_s	N_s/N_b	N_{ss}
200 GeV	2.91	1.65	875	1.77	39.3
400 GeV	3.44×10^{-1}	0.818	103	0.422	6.06
800 GeV	9.4×10^{-3}	0.2	3	0.047	0.364

Table 5.8: MSSM Higgs production via gluon fusion $gg \rightarrow \phi^0\phi^0 \rightarrow b\bar{b}\tau^+\tau^- \rightarrow b\bar{b}lj_\tau + \not{E}_T$ at $\sqrt{s} = 14\,TeV$ for $\mathcal{L} = 300(3000)fb^{-1}$. These values are calculated for $tan\,\beta = 50$, and all cross section values are in fb.

Chapter 6

Trilinear Higgs Coupling

Besides measuring basic properties of newly discovered particles such as mass, decay width, branching ratios and spin-parity, it is really important to measure its couplings. Precise determination of Higgs couplings to fermions, gauge bosons and the Higgs itself, are a few of the most important experimental challenges for future experiments. Higgs self couplings are more important in order to reconstruct the Higgs potential and hence to confirm the mechanism of EWSB(Electro Weak Symmetry Breaking). The Higgs potential in the effective Lagrangian can be written as,

$$V(\phi) = -\mu^2(\phi^\dagger \phi) + \frac{1}{2}\lambda(\phi^\dagger \phi)^2 \tag{6.1}$$

Where $\lambda = \frac{M_h^2}{v^2}$ and $\mu^2 = \frac{M_h^2}{2}$. M_h is the Higgs mass; v is the vacuum expectation value, and ϕ is the Higgs field. This Higgs potential basically depends on m_h and v, $v = (\sqrt{2}G_F)^{-\frac{1}{2}} \cong 246$ GeV, and G_F is Fermi constant, which was measured over 80 years ago. The SM Higgs mass, m_h, was measured few years ago by the ATLAS and CMS collaborations at the LHC. It was found that $m_h = (125.09 \pm 0.24)$ GeV[3][4]. Rewriting the Higgs potential in terms of physical Higgs boson leads to the trilinear Higgs coupling which is defined as,

$$\lambda_{hhh}^{SM} = -\frac{3m_h^2}{v} \tag{6.2}$$

The next experimental challenge remaining is to measure the Higgs self couplings in order to verify the Higgs potential. Both the trilinear Higgs coupling(λ_{hhh}) and

the quartic coupling(λ_{hhhh}) should be measured independently to determine the Higgs potential accurately. λ_{hhh} can be measured at the LHC via Higgs pair production processes explained earlier in this dissertation. In the next section, we will be discussing the possibility of measuring the trilinear Higgs coupling with the improved cross section values presented here. However, measuring Higgs self couplings are not an easy task at the LHC because of small cross section values and large backgrounds in the $gg \to hh$ process. Measuring couplings between three physical Higgs bosons is a priority for the proposed linear e^+e^- collider (ILC), and we will also initiate the study of Higgs production via electron positron collision.

6.1   Measuring the Trilinear Higgs coupling at LHC

As we see in Fig. 2.1 , Higgs pair production from gluon fusion involves trilinear Higgs self couplings in its triangle diagram and in the b quark fusion . Recently many groups [42] [43] [44] [34] [24] have carried out several phenomenological studies about the possibility of determining the Higgs boson self-coupling at hadron colliders. In this study, we will be discussing the possibilities of measuring trilinear Higgs coupling at the LHC using the cross sections evaluated for Higgs pair productions discussed in this thesis so far. Higgs pair production from gluon fusion via box and triangle diagrams are dominant production channels to be considered towards measuring the trilinear Higgs self coupling at LHC. Though only the triangle diagram contains the self coupling in it, the interference of the two amplitudes is sensitive to the hhh coupling. Cross sections for Higgs pair production are presented in Fig 6.1 as a function of κ,

for three different center of mass energies. κ is the ratio of trilinear Higgs coupling to

the standard Model trilinear higgs coupling given by equation 6.2, which is,

$$\lambda_{hhh} = \kappa \ \times \ \lambda_{hhh}^{SM}. \tag{6.3}$$

In Figure 6.1, the cross sections are plotted as a function of κ for three different

center of mass energies. As can be seen from the plot at $\kappa \approx 2.5$, the cross section has

a minimum value due to the complete destructive interference from the two Feynman

diagrams box and triangle. Though the shape of this curve looks the same for all

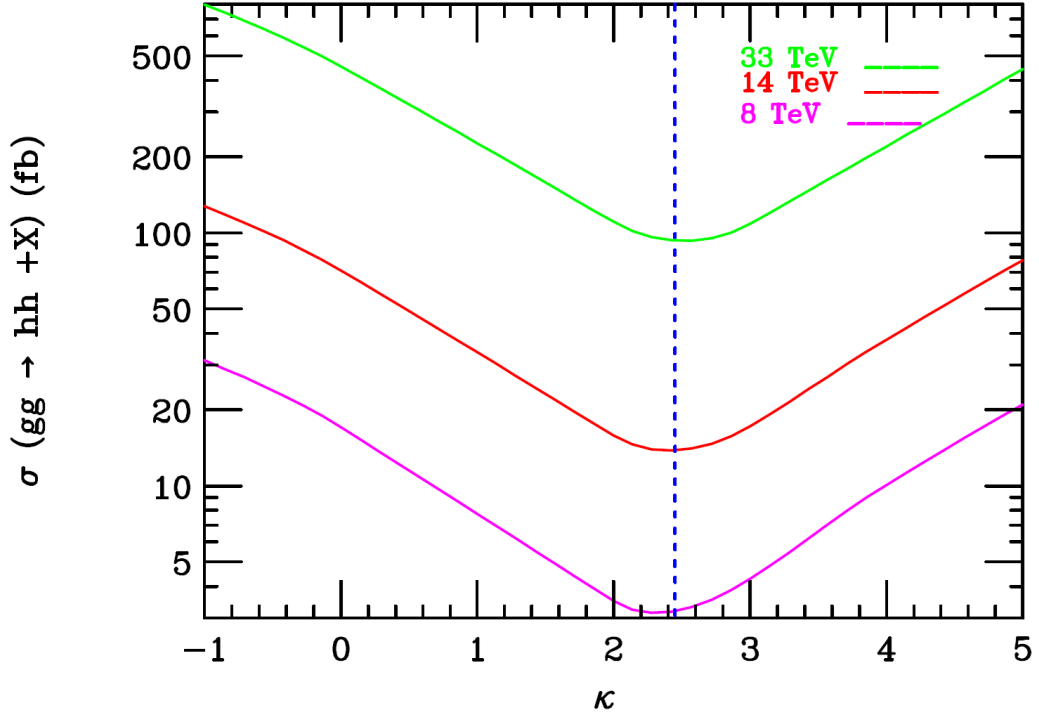channels, the minimum locates in different κ values depending on the channel [24].

Figure 6.1: NLO(LO+kfactor(1.88)) cross sections for Higgs pair production via $gg \to hh$ as a function of κ for three different energies. No Higgs decay is considered here.
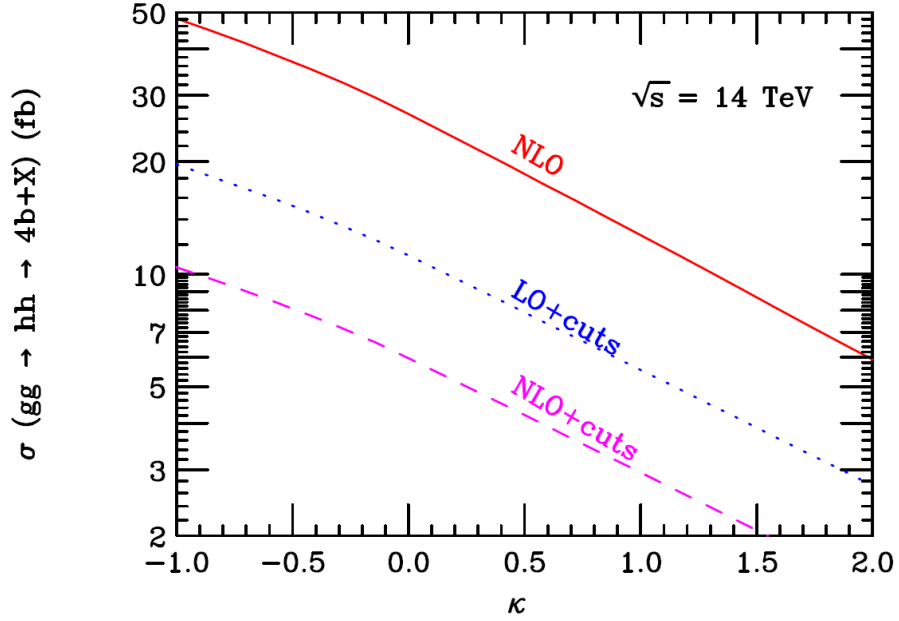
Figure 6.2: Cross section of $gg \to hh \to (b\bar{b})(b\bar{b})$ as a function of κ. The red solid line shows the NLO cross section without any cuts, the blue dotted line shows LO cross section with cuts, and the dash magenta line shows NLO cross section including all cuts for the final state particles.

Figure 6.2 shows the total NLO and LO cross sections for the process $gg \to hh \to (b\bar{b})(b\bar{b})$ for the center of mass energy of 14 at LHC calculated for different κ values. The selection cuts we applied here are the same as explained in the 2nd and the 4th chapters.

The variation of significance as a function of κ is presented in Fig. 6.3 for L=30 fb^{-1} and $300fb^{-1}$. The significance decreases as $\kappa = \lambda_{hhh}/\lambda_{hhh}^{SM}$ increases due to a reduction in the cross section. The significance for $\bar{b}\bar{b}b\bar{b}$ is greatly enhanced here by introducing the mass cut which reduces a large amount of QCD backgrounds associated with the
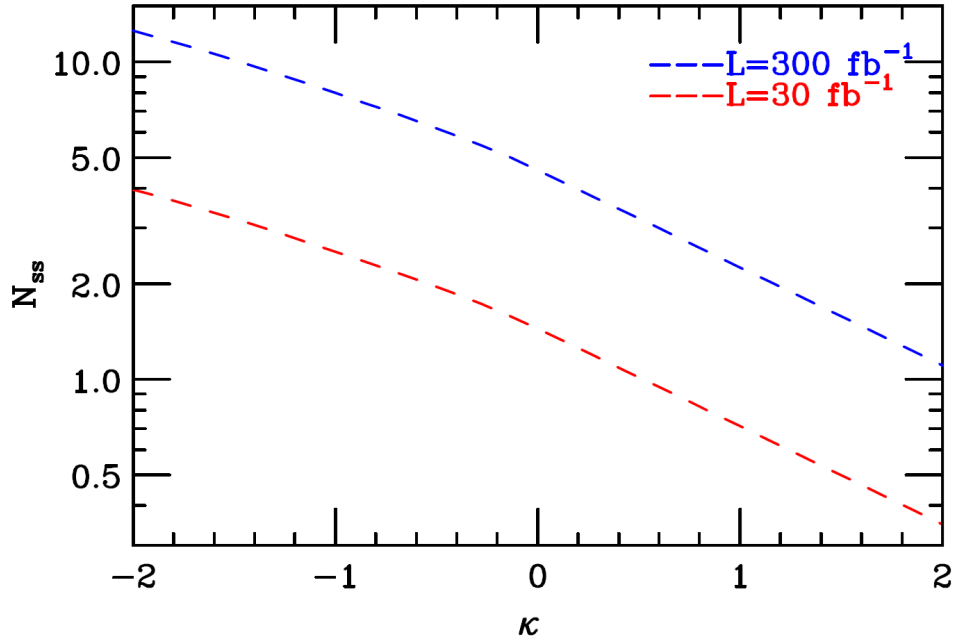
Figure 6.3: The calculated significances for the SM Higgs pair production
via $gg \rightarrow hh \rightarrow (b\bar{b})(b\bar{b})$ for different values of κ at 3000 fb^{-1} for 14 TeV
at the LHC.

$b\bar{b}b\bar{b}$ final state. For $\kappa = 1$ significance is 6.94 for the luminosity of 3000 fb^{-1}. Also,

as presented in Chapter 5, the $b\bar{b}\tau^+\tau^- \rightarrow b\bar{b}lj_\tau$ has a significance of 7.7. With these

results, we can claim that both of these channels have positive constraints towards

measuring the trilinear Higgs coupling at 14 TeV LHC with integrated luminosity

of 3000 fb^{-1}. Reference [34] claims that one can set a limit for $\lambda \leq 1.2$ at 95% CL

for $b\bar{b}b\bar{b}$ final state at 3000 fb^{-1}. Reference [24] concludes that $b\bar{b}\tau^+\tau^-$ is a promising

channel to start real experimental analysis to probe the trilinear Higgs coupling at

LHC through Higgs pair production. The results of this study also verify the same

fact even with high acceptance for $b\bar{b}b\bar{b}$ final state.

6.2 Measuring Trilinear Higgs coupling at ILC

Lepton colliders are well known for high precision measurements. Measuring the tri-linear Higgs coupling will be one of the main focuses for the next proposed $e^+ e^-$ machine, the International Linear collider(ILC). The ILC is an electron positron collider and is planned to have a collision energy in the range 500 GeV - 1 TeV. This will initially run at energies $\sqrt{s} = 200 - 500$ GeV with an integrated luminosity of 500 fb^{-1} [45] TDR-ILC. More details about the design and expected upgrades can be found in [46] [47]. Even though the collision energy for the LHC is higher than that of the ILC, measurements are expected to be more accurate at the ILC with higher luminosity.

In this study, we focus on the Higgs pair production at the ILC via $e^+ e^-$ collisions -three major processes of Higgs production were studied here to explore the trilinear Higgs couplings. We assume that κ is a free parameter which is in the range $0.5 \leq \kappa \leq 2$.

Variation of cross sections was studied as a function of κ and for the collision energy changing from 500 GeV to 2 TeV using a Monte Carlo program with the amplitudes calculated by MadGraph5. Cross sections were also calculated directly from MadGraph5 for comparison purposes. Numerical values given here are calculated at the mass of the SM Higgs boson(126 GeV).
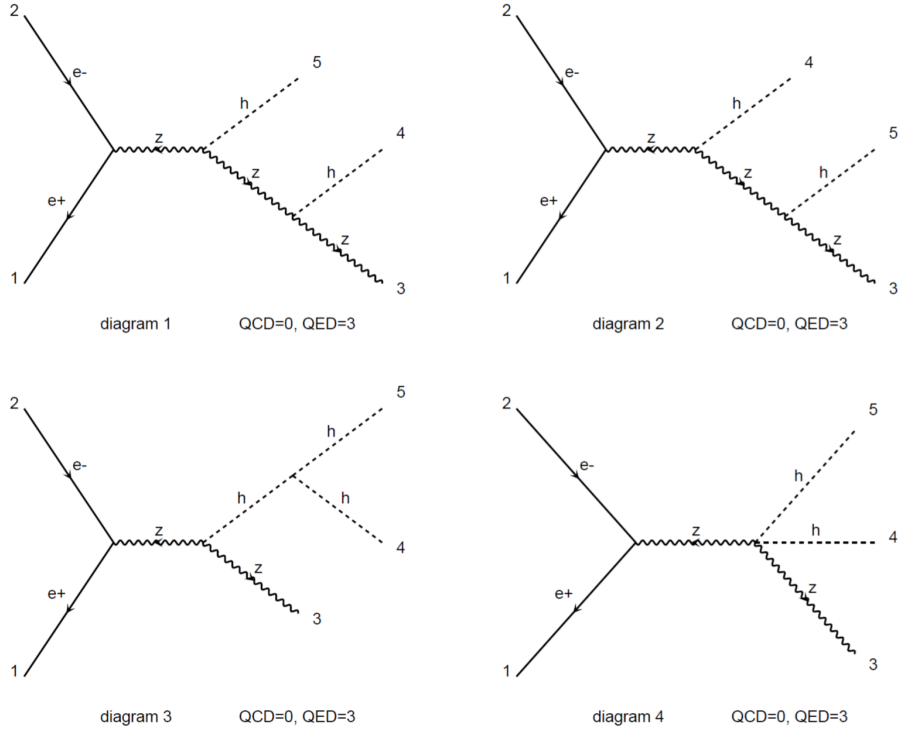
Figure 6.4: Feynman diagrams produced by MadGraph5 for the process $e^+e^- \rightarrow Zhh + X$. Diagram 3 involves trilinear Higgs self coupling.

6.2.1 $e^+e^- \rightarrow Zhh + X$

$e^+e^- \rightarrow Zhh$ is one of the major processes to produce two Higgs at electron positron colliders. Several studies have been done discussing the possibility of measuring the trilinear Higgs self coupling through this process at the ILC [48][49][50]. Fig. 6.4 shows the Feynmann diagrams for the double Higgs strahlung process $e^+e^- \rightarrow Zhh + X$ which includes one diagram with the trilinear Higgs coupling and three other diagrams which do not include self coupling. We studied the cross sections as a function of κ for different center of mass energies. Fig. 6.5 presents the calculated cross sections for center of mass energies of 500 GeV, 1000 GeV and 2000 GeV. The red dashed line

shown here is for the contribution over diagram 1, 2 and 4 which does not contribute to the trilinear Higgs coupling and is a constant over the ratio of $\lambda_{hhh}/\lambda_{hhh^{SM}}$. Blue dashed line is for the 3rd diagram which has trilinear couplings in it, and the solid line represents the total cross section for all 4 diagrams.

6.2.2 $e^+e^- \rightarrow hh\nu_e\nu_e + X$

$e^+e^- \rightarrow \nu_e\overline{\nu_e}hh$ is also considered to be a dominant process for Higgs production which probes the Higgs self coupling. Higgs production via double-Higgs strahlung at linear colliders has been discussed in past studies [24] [48]. All possible Feynmann diagrams for the process $e^+e^- \rightarrow \nu_e\overline{\nu_e}hh + X$ via W and Z bosons are included in the Appendix E. There are two diagrams with the trilinear Higgs coupling and six other diagrams which have no self coupling. The contribution from WW fusion is higher compared to ZZ, but here we consider combined results from both. Fig. 6.7 shows the cross section for the process as a function of $\kappa = \lambda_{hhh}/\lambda_{hhh}^{SM}$.

6.2.3 $e^+e^- \rightarrow hhe^+e^- + X$

As stated in Fig. 6.8, production cross sections of Higgs via $e^+e^- \rightarrow hhe^+e^- + X$ were studied as a function of κ. All possible Feynman diagrams made by MadGraph5 can be find in the Appendix E.

6.2.4 Summary

The production cross sections for the processes Zhh, $\nu_e\overline{\nu_e}hh$ and hhe^+e^- as a function of center of mass energy at the Higgs mass of 126 GeV are given in Fig. 6.6. As can be
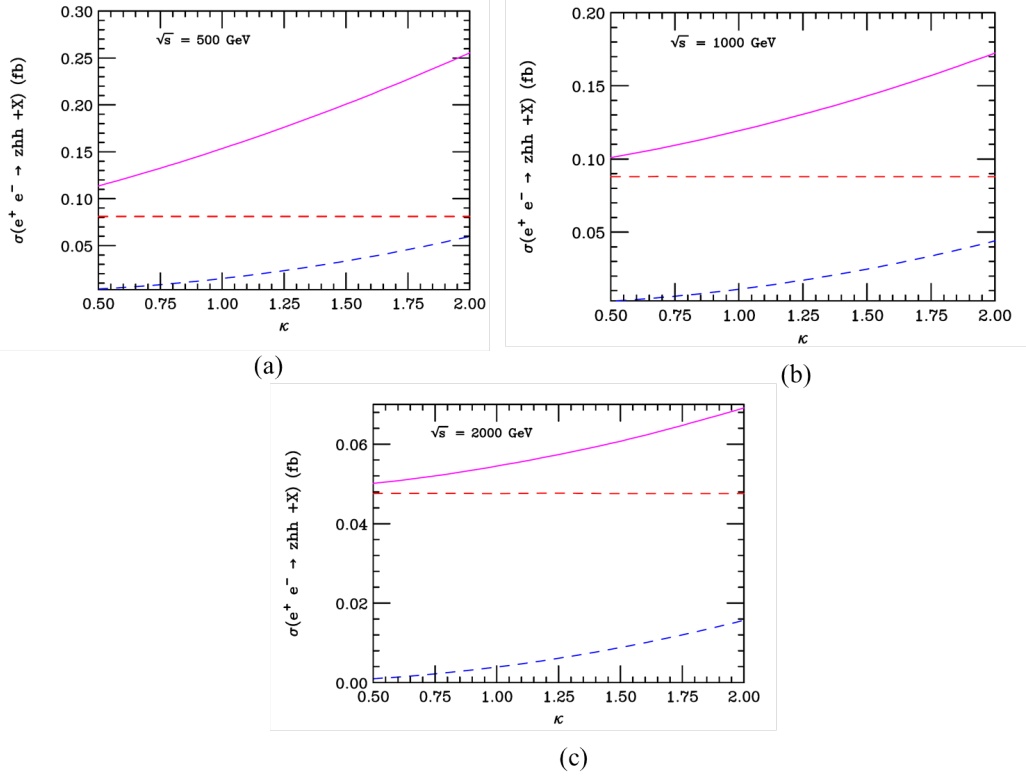
(a)

(b)

(c)

Figure 6.5: Cross section of Higgs pair production for the process $e^+e^- \rightarrow Zhh + X$ as a function of κ. Solid (magenta) represents the total cross section; red dashed line represents the contribution of diagrams with no trilinear Higgs vertex, and blue dashed line represents the contribution of diagrams with trilinear Higgs vertex.
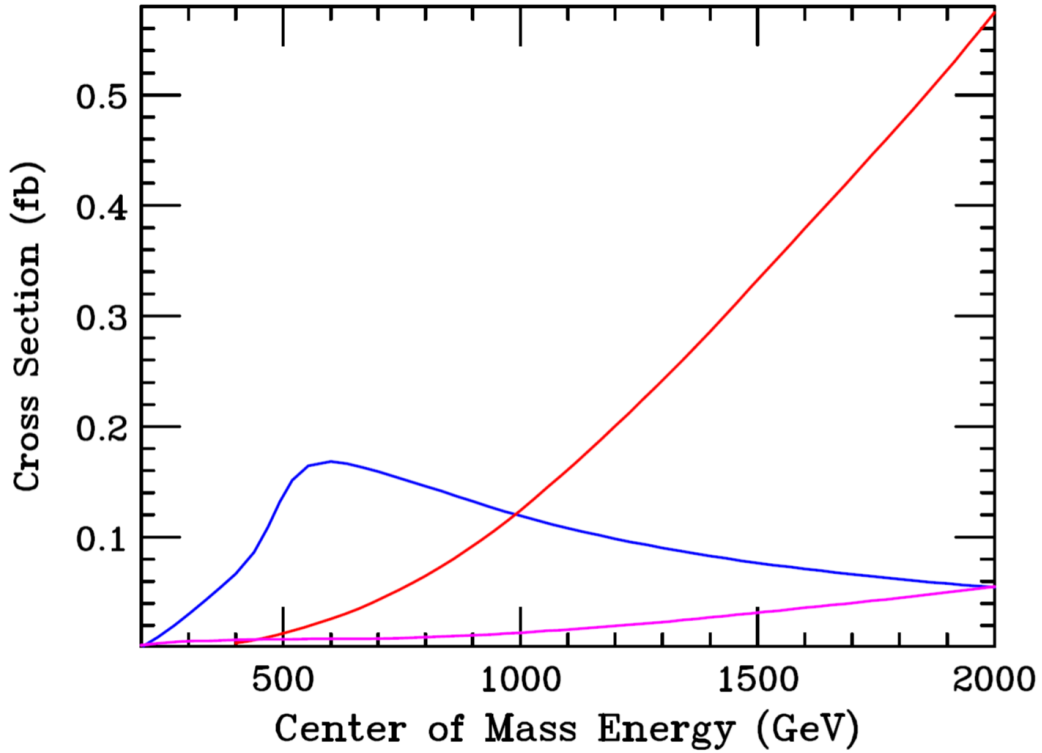
Figure 6.6: Cross sections of three major Higgs production processes at the ILC as a function of $\sqrt{s}$. The blue solid line represents zhh final state, the red line represents $\nu_e\nu_ehh$ final state and the magenta line represents e^+e^-hh final state.

seen from the figure, the $e^+e^- \rightarrow Zhh+X$ process gives higher cross sections for lower energies around 500 GeV while $e^+e^- \rightarrow \nu\bar{\nu}hh+X$ gives higher cross sections at higher center of mass energies. The process $e^+e^- \rightarrow hhe^+e^- + X$ gives comparably lower cross sections compared to the other two processes. However, the combination of all these processes gives significantly large cross sections for overall center of mass energies. Though the cross sections produced here are smaller than the cross sections produced at the LHC, for example in gluon fusion, the ILC processes are still promising since

they are not covered by the large backgrounds as in LHC. As emphasized in [48] and [49], there is a possibility of measuring the trilinear Higgs self coupling even with the center of mass energy of 500 at the ILC with high luminosities.
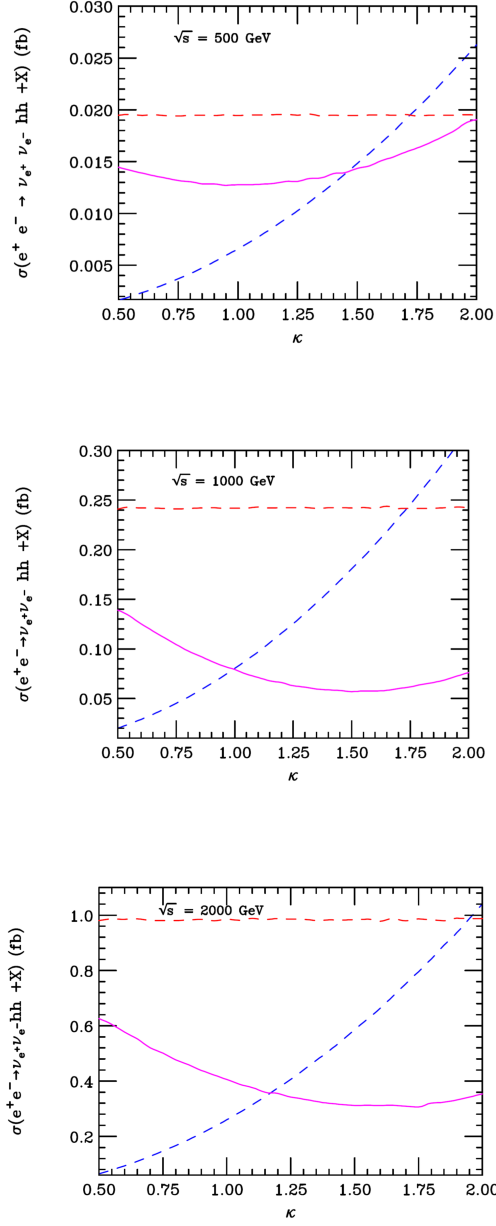
Figure 6.7: Cross section of Higgs pair production for the process $e^+e^- \to \nu_e \nu_e hh + X$ as a function of κ. The solid (magenta) line represents the total cross section; the red dashed line represents the contribution of diagrams with no trilinear Higgs vertex, and the blue dashed line represents the contribution of diagrams with a trilinear Higgs vertex.

Figure 6.8: Cross section of Higgs pair production for the process $e^+e^- \to e^+e^-hh + X$ as a function of κ. The solid (magenta) line represents the total cross section; the red dashed line represents the contribution of diagrams with no trilinear Higgs vertex, and the blue dashed line represents the contribution of diagrams with trilinear Higgs vertex.
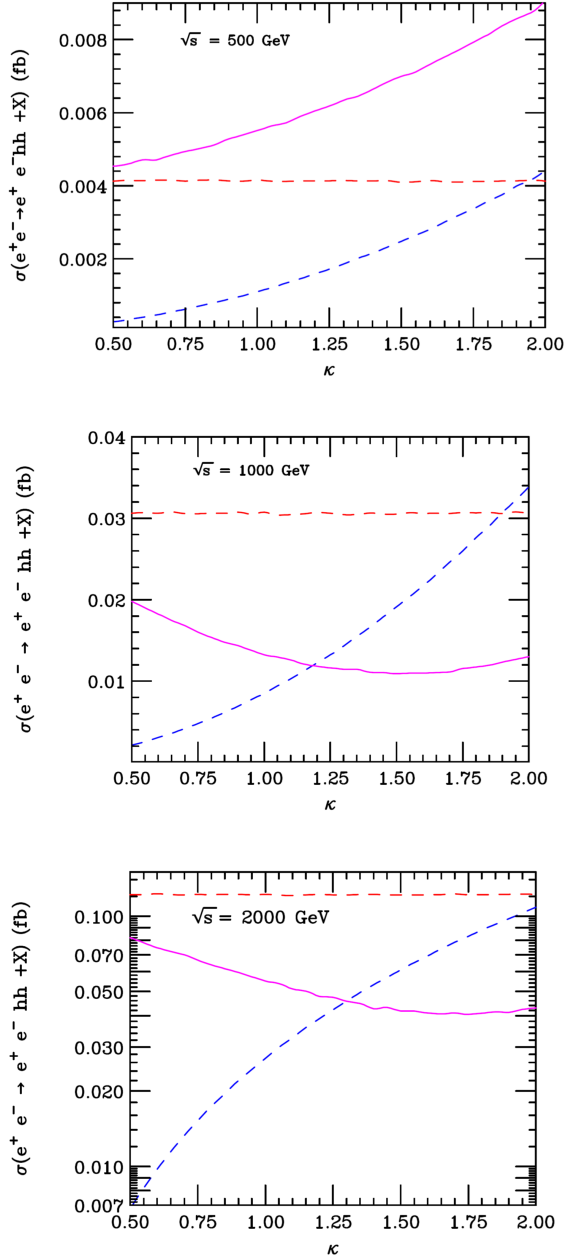
65

Chapter 7

Summary and Conclusion

In the literature, there are numerous studies done on Higgs production through several channels. Though Higgs decays into b jets carry the highest branching ratio, this channel was not of interest due to high QCD backgrounds, and $b\bar{b}\tau^-\tau^+$ was the next promising channel to consider for future targets, like measuring Higgs self couplings. In this study, we evaluated some important cross sections for measuring the trilinear Higgs couplings at the LHC. The processes we considered here were $pp \to hh \to b\bar{b}b\bar{b} + X$ and $pp \to hh \to b\bar{b}\tau^+\tau^- \to b\bar{b}lj_\tau + \not{E}_T$ for both the SM and the MSSM via gluon fusion and b quark fusion. Using a new method of mass cuts on the $b\bar{b}b\bar{b}$ final state, we could reduce 90% of background while saving 80% of the signal. For the SM, this improved the ratio of signal vs background significantly which could lead to measurements of the trilinear Higgs couplings at the LHC in future, probably at $\sqrt{s} = 14\,\text{TeV}$.

In the MSSM, b quark fusion is especially interesting because the couplings and, hence the signal, can be greatly enhanced with large values of $tan\,\beta$. Neutral Higgs production via b quark fusion was studied, and with the updated mass cut for the $4b$ final state, we could get $N_{ss} = 2.87(9.0)$ with signal events of 2562(25620) for the integrated luminosity $=300(3000)fb^{-1}$, at $\sqrt{s} = 14\,\text{TeV}$ for a pseudo scalar mass of 200 GeV and for $tan\,\beta = 50$. We also evaluated the $b\bar{b}\tau^+\tau^-$ final state followed by $\tau^+\tau^- \to lj_\tau + \not{E}_T$ both via gluon fusion and b quark fusion. With the selection cuts applied to the reconstructed mass of Higgs from $\tau^+\tau^-$, the cross section rates were

improved and hence the significance.

The results presented in this study conclude that gluon fusion with a $(b\bar{b})(b\bar{b})$ final state places a high constraint on measuring the trilinear Higgs couplings in the SM at the LHC running at 14 TeV. SM Higgs pair production via gluon fusion was studied here with the ratio of Higgs self couplings (κ). For $\kappa = 1$, a statistical significance of 6.9 (with 137 events for the signal) and 7.7 (with 180 events for the signal) was obtained for $b\bar{b}b\bar{b}$ final state and the $b\bar{b}\tau^+\tau^- \rightarrow b\bar{b}lj_\tau$ final state respectively with integrated luminosity of 3000 fb^{-1} at the LHC 14 TeV. With these results, we can claim that there is a high possibility of measuring the trilinear Higgs self coupling at the LHC through these two channels. However, for a precise measurement of trilinear Higgs couplings, we also investigated the possible processes for measuring it at the proposed electron positron linear collider, the ILC, in the future.

References

[1] J. F. Gunion, H. E. Haber, G. Kane, and S. Dawson, *The Higgs Hunter's Guide* (Perseus, Cambridge, MA, 2000).

[2] The Noble Prize in Physics 2013.

[3] ATLAS collaboration, G. Aad, *et al.*, Phys. Lett. B **716**, 1 (2012).

[4] CMS collaboration, S. Chatrchyan, *et al.*, Phys. Lett. B **716**, 30 (2012).

[5] C. N. Yang and R. L. Mills, Physical Review **96**, (1954).

[6] P. W. Higgs, Phys. Rev. Lett **13**, 508 (1964).

[7] F. Englert and R. Brout, Phys. Rev. Lett **13**, 321 (1964).

[8] G. S. Guralnik, C. Hagen, and T. Kibble, Phys. Rev. Lett **13**, 585 (1964).

[9] H. E. Haber, arXiv:hep-ph9306207 **1**, (1993).

[10] H. E. Haber, Introductory low-energy supersymmetry.1993.

[11] S. P. Martin, A Supersymmetry Primer.1997.

[12] H. E. Haber, G. L. Kane, and T. Sterling, Nucl. Phys. B **3**, 493 (1979).

[13] L. Hall and M. Wise, Nucl. Phys. B **187**, 397 (1981).

[14] S. L. Glashow and S. Weinberg, Phys. Rev. D **15**, 1958 (1977).

[15] J. F. Donoghue and L.-F. Li, Phys. Rev. D **19**, 945 (1979).

[16] S. Dawson, S. Dittmaier, and M. Spira, ArXiv:hep-ph **1**, (1998).

[17] E. Glover and J. van der BIJ, Nucl. Phys. B **309**, 282 (1988).

[18] T. Plehn, M. Spira, and P. Zerwas, Nucl. Phys. B .

[19] D. A. Dicus, C. Kao, and S. S. D. Willenbrock, Phys. lett. **203**, (1987).

[20] D. de Florian and J. Mazzitelli, Phys. Rev. lett. **111**, (2013).

[21] A. Martin, R. T. W.J.Stirling, and G. Watt, Eur. Phys J. **C 63**, 189 (2009).

[22] G. Passarino and M. Veltman, Nucl. Phys **160**, 150 (1979).

[23] J. Kuipers, T. Ueda, J. Vermaseren, and J.Vollinga, comput. Phys. Commun. **184**, 1453 (2013).

[24] J. Baglio *et al.*, arXiv:1212.5581v2[hep-ph] **2**, (2013).

[25] V. D. Barger, , and R. J. Philips, *Collider Physics Updated Edition* (Westview Press, ADDRESS, 1996).

[26] S. Heinemeyer, W. Hollik, and G. Weiglein, arXiv:hep-ph/981232001 **1**, (1998).

[27] S. Dawson, C. Kao, Y. Wang, and P. Williams, Physical Review D **75**, (2007).

[28] S. Dawson, C. Kao, and Y. Wang, Physical Review D **77**, (2008).

[29] D. Dicus and S. Willenbrock, Phys. Rev. D **39**, (1989).

[30] D. Dicus, T. Stelzer, Z. Sullivan, and S. Willenbrock, Phys. Rev. D **59**, (1999).

[31] C. Balazs, H. He, and C. P. Yuan, Phys. Rev. D **60**, (1999).

[32] C. Kao, S. Sachithanandam, J. Sayre, and Y. Wang, arXiv:0908.1156[hep-ph] **2**, (2009).

[33] C. Kao, D. A. Dicus, R. Malhotra, and Y. Wang, arXiv:0711.0232[hep-ph] **1**, (2007).

[34] D. E. F. de Lima, A. Papaefstathiou, and M. Spannowsky, arXiv:1404.7139v2[hep-ph] **2**, (2014).

[35] J. M. Butterworth, A. R. Davison, M. Rubin, and G. P. Salam, Phys.Rev. Lett **100**, (2008).

[36] F. Maltoni and T. Stelzer, JHEP 2 (2003).

[37] K. Yang, Phd. thesis, University of Oklahoma, 2013.

[38] J. M. Campbell, R. K. Ellis, F. Maltoni, and S. Willenbrook, Phys. Rev. D **69:074021**, (2004).

[39] R. Bonciani, S. Catani, M. L. Mangano, and P. Nason, Nucl. Phys. **B529**, 424 (1998).

[40] P. Nason, S. Dawson, and R. K. Ellis, Nucl. Phys. **B303**, 607 (1988).

[41] S. Zhu, Phys. Lett **B 524**, 283 (2002).

[42] U. Baur, T. Plehn, and D. Rainwater, Physical Review D **67**, (2003).

[43] F. Geortz, A. Papaefstathiou, L. L. Yang, and J. F. Zurita, arXiv:1309.3805v1[hep-ph] (2013).

[44] V. Barger, L. L. Everett, C. B. Jackson, and G. Shaughnessy, arXiv:1311:2931 **1**, (2013).

[45] C. Adolphson *et al.*, arXiv:1306.6353 **1**, (2013).

[46] H. Baer, T. Barklow, K. Fujii, Y. Gao, A. Hoang, *et al.*, **2:Physics**, (2013).

[47] T. Behnke *et al.*, **4**, (2013).

[48] D. J. Miller and S. Moretti, Eur. Phys. J.] **C 13**, 459 (2000).

[49] A. Djouadi, W. Kilian, M.Muhlleitner, and P. Zerwas, hep-ph9903229 (1999).

[50] J. Tian and K. Fujii, arXiv:1311.6528v1[hep-ph] **1**, (2013).

Appendix A
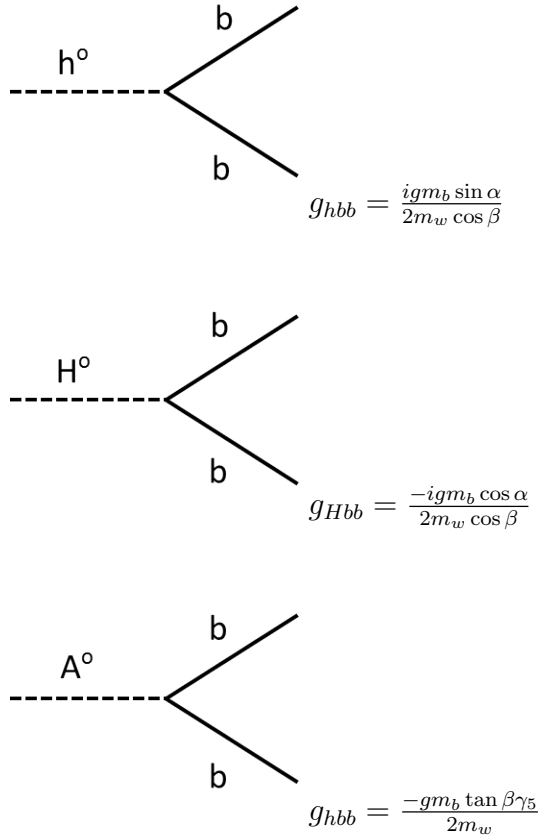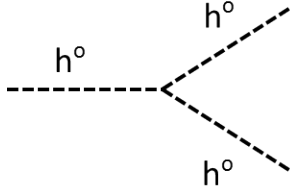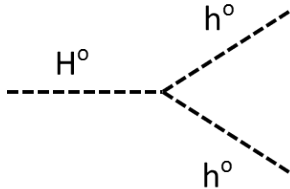
Higgs Couplings to quarks in MSSM

Figure A.1: Feynman rules for Higgs-quark-quark vertices. Where g is the standard SU(2) gauge group coupling; m_w is mass of W boson; m_b is mass of the b quark, and α is Higgs mixing angle [1].

Appendix B
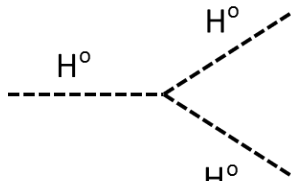
Trilinear Higgs couplings among MSSM neutral Higgs

$$g_{hhh} = \frac{-3igm_z \cos 2\alpha \sin (\alpha+\beta)}{2\cos \theta_w}$$
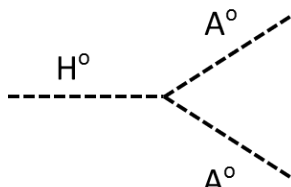

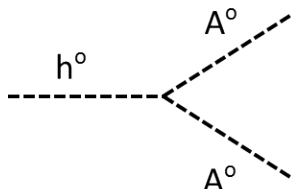$$g_{Hhh} = \frac{-igm_z (2\sin 2\alpha \sin (\alpha+\beta) - \cos (\beta+\alpha) \cos 2\alpha)}{2\cos \theta_w}$$

$$g_{hHH} = \frac{igm_z (2\sin 2\alpha \cos (\alpha+\beta) + \sin (\beta+\alpha) \cos 2\alpha)}{2\cos \theta_w}$$

H°

H° ⟍
   ⟍

H° ⟋
   ⟋

$$g_{HHH} = \frac{-3igm_z \cos 2\alpha \cos{(\alpha+\beta)}}{2\cos\theta_w}$$

H°

A° ⟍
   ⟍

A° ⟋
   ⟋

$$g_{hAA} = \frac{-igm_z \cos 2\beta \sin{(\alpha+\beta)}}{2\cos\theta_w}$$

h°

A° ⟍
   ⟍

A° ⟋
   ⟋
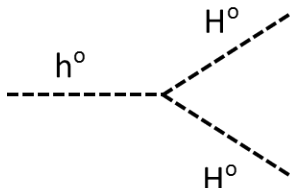
$$g_{HAA} = \frac{igm_z \cos 2\beta \cos{(\alpha+\beta)}}{2\cos\theta_w}$$

Figure B.1: Higgs self couplings for the MSSM, where g is the standard SU(2) gauge group coupling; m_w is mass of W boson; m_b is mass of the b quark, and α is Higgs mixing angle, β is free parameter in mssm[1] .

Appendix C

Input parameters for the FeynHiggs

Here are the input parameters we set in file "var.in" to calculate masses and couplings of the cp-even neutral Higgs bosons in the MSSM[26].

$MT = 173.5$: Mass of top quark

$MSusy = 2000.$: A generic soft-SUSY breaking mass

$MA0 = 1000.0$: The CP odd Higgs mass

$Abs(M_2) = 389.$: The SU(2) gaugino mass parameter

$Abs(MUE) = 1000.$: The Higgs mixing parameter

$TB = 50.0$: tan(beta)

$Abs(Xt) = 4899.$: Alternative stop mixing parameter

$Abs(M_3) = 1100.$: The gluino mass parameter

Appendix D

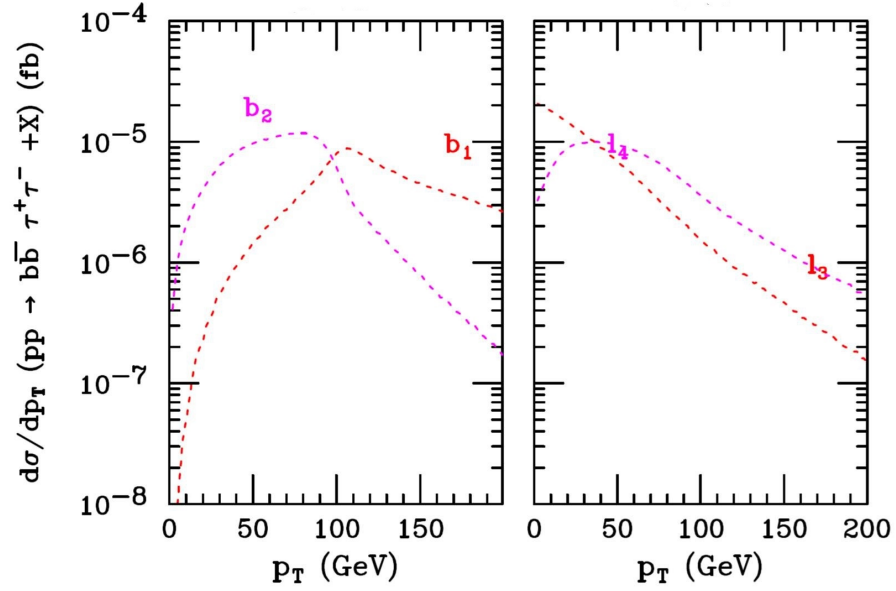# Distributions for production of psudoscalar pair via gluon fusion with the $b\bar{b}lj_\tau$ final state.

Figure D.1: Transverse momentum distribution for $b\bar{b}lj_\tau$ from gluon fusion for MSSM via a pair of pseudo scalars.
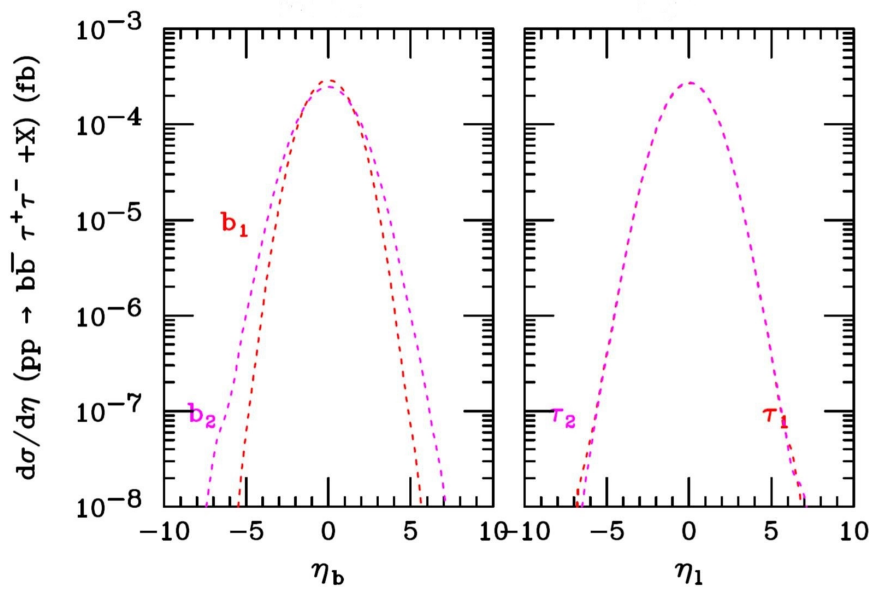
Figure D.2: Distribution of pseudo rapidity for the final state $b\bar{b}lj_\tau$ for the production of pseudoscalars via gluon fusion.
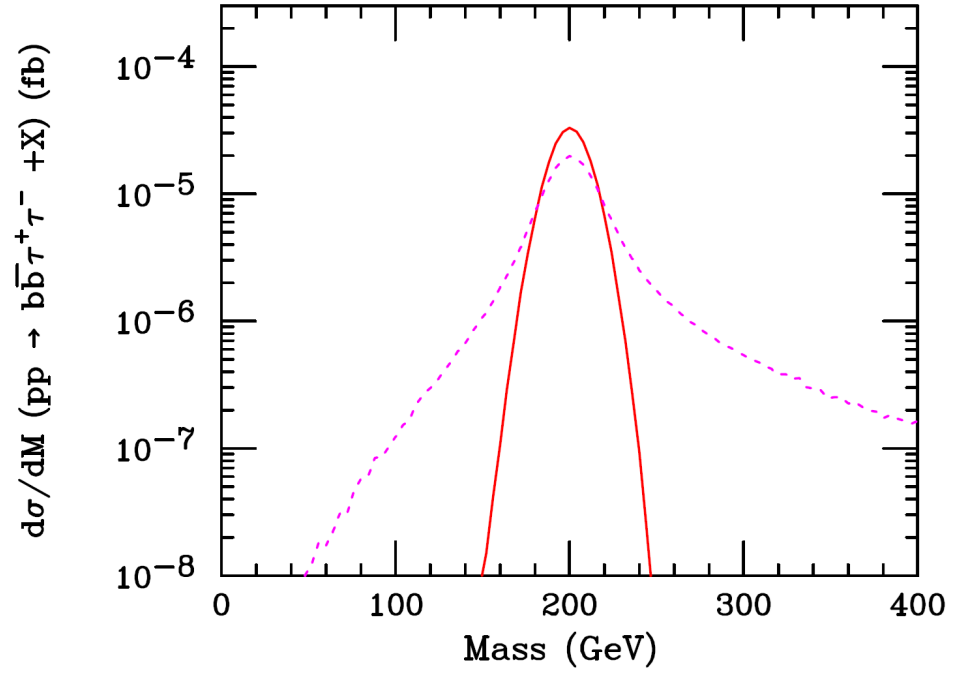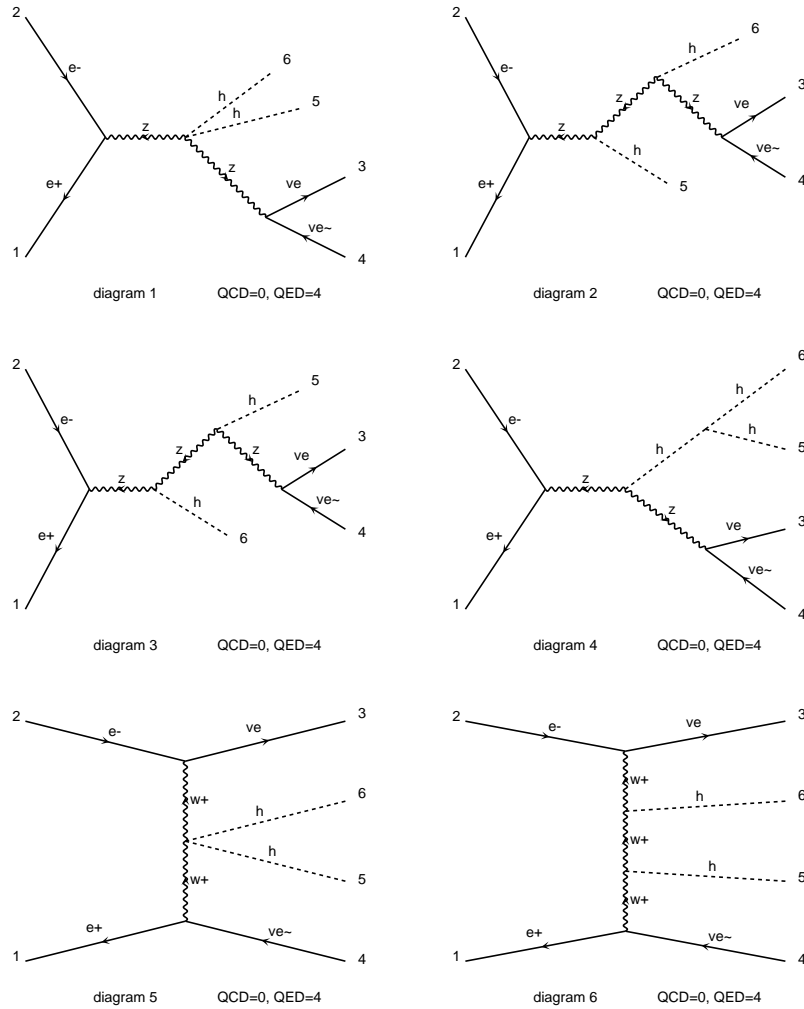
Figure D.3: Distribution of invariant mass between final state for the production of pseudoscalars via gluon fusion; red line is invariant mass between $b\bar{b}$, and dashed magenta represents the invariant mass between lj_{τ}.

Appendix E

Feynman Diagrams of the process $e^+e^- \rightarrow \nu\nu hh + X$

Figure E.1: Feynman diagrams made by MadGraph5 for the Higgs production at ILC via $e^+e^- \rightarrow \nu\nu hh + X$.